

## Structural Features and Tribological Properties of Multilayer Coatings Based on Refractory Metals

A. D. Pogrebnjak<sup>a, \*</sup>, Ya. O. Kravchenko<sup>a, b</sup>, O. V. Bondar<sup>a</sup>,  
B. Zhollybekov<sup>c</sup>, and A. I. Kupchishin<sup>d</sup>

<sup>a</sup>Department of Nanoelectronics, Sumy State University, Sumy, 40007 Ukraine

<sup>b</sup>NanoBioMedical Center, Adam Mickiewicz University of Poznan, Poznan, Poland

<sup>c</sup>Berdakh Karakalpak State University, Nukus, Uzbekistan

<sup>d</sup>Abay Kazakh National Pedagogical University, Almaty, Kazakhstan

\*e-mail: alexp@i.ua

Received March 1, 2017

**Abstract**—A comparative analysis of the structural features and tribological properties of multilayer coatings based on refractory metal compounds has been conducted in this review. Features of formation of the electronic structure of the synthesized coatings have been discussed, and the effect of methods and conditions of deposition on changes in the physicomechanical characteristics of nanocrystalline structures based on transition metal nitrides has been shown. Dependences of antifriction properties, corrosion resistance, and thermal stability on the modulation period ( $\Lambda$ ) and the number of bilayers in the studied multilayer coatings have been determined. A decrease in the modulation period of individual layers in a coating positively affects the oxidation resistance of the coating, while an increase in the number of interfaces between the layers slows down the diffusion of oxygen atoms deep into the coating and, thereby, increases the protective properties of the multilayer system as a whole. The effect of the droplet component in cathodic-arc coatings on corrosion development mechanisms in corrosive media has been shown. A class of multifunctional multilayer coatings with an adaptive friction mechanism, which is characterized by a change in the properties and structure during tribological tests, has been discussed separately.

**Keywords:** multilayer coatings, thermal stability, coefficient of friction, corrosion resistance, wear

**DOI:** 10.1134/S2070205118020107

### INTRODUCTION

Titanium nitride coatings prepared by physical vapor deposition (PVD) on high-speed steel were shown proven to exhibit fairly high wear resistance as far back as the 1980s. However, at present, these coatings no longer provide high performance in the protection of cutting tools operating under extreme conditions. Nanocomposite coatings exhibiting superhigh hardness ( $\geq 45$  GPa) and oxidation resistance at temperatures of about 1000°C have been synthesized. However, these coatings are characterized by a relatively high coefficient of friction at high temperatures, a feature that hinders their practical application. Over the past decade, the scientific community has tried various ways to improve and modify protective coatings. A common goal of all the studies is the formation of a universal multifunctional material with reproducible physicomechanical and tribological characteristics. The formation of multilayer systems of multiply repeating bilayers of transition metal nitrides in order to impart a wide range of properties to the resulting

coating is an approach to further improving nitride coatings.

Another way to improve the characteristics of functional coatings is the formation of a kinetically and thermodynamically stable solid solution comprising at least five elements in the coating. This class of metallic compounds is commonly referred to as “high-entropy alloys” (HEAs). The combination of HEA layers and layers of other refractory elements into bilayers is also of particular scientific interest.

This brief review summarizes results of studies of the structural features and phase composition of multilayer nanocomposite coatings and their effect on the physicomechanical and tribological properties of the coatings. Coatings based on an extended group of period 3–6 refractory metals prepared by magnetron sputtering and vacuum-arc deposition are discussed. The dependences of the hardness, as well as of the wear and friction resistance, on the structure, thickness, and number of bilayers in multilayer nanocomposite systems are analyzed. Analysis of the literature shows that the wear resistance of many multilayer

nitride coatings (TiAlN/VN [1], TiN/CrN [2], TiN/Nb [3]) is higher than that of the commonly used single-layer TiN coatings. This review is focused on the morphology and tribological properties of multilayer nitride coatings.

#### SUMMARY OF METHODS OF PREPARATION OF MULTILAYER NANOCOMPOSITE SYSTEMS AND THEIR STRUCTURAL FEATURES

The authors of many studies focusing on surface-structure engineering and generation of vacuum condensates [4–7] have indicated the key role played by methods and conditions for coating preparation. Multilayer coatings can be prepared by a variety of currently available methods, such as thermal evaporation, laser ablation, vacuum-arc deposition, ion-beam sputtering, and magnetron sputtering. Magnetron sputtering and vacuum-arc deposition are the most commonly used PVD methods for the formation of multilayer nitride coatings. These methods make it possible to control the structural state of each of the layers separately via selecting the layer thickness, the type of the material constituting the layer, and the number of layers in the period and, thereby, provide the formation of structures with unique tribological properties.

Magnetron sputtering has the following advantages:

- high degree of chemical purity of the resulting coatings;
- deposition of coatings on substrates with a large area and a fairly complex geometric shape;
- conditions excluding the substrate heating; and
- significantly higher adhesion strength of the coating to the substrate and between the layers than the adhesion strength of similar coatings prepared by thermal vacuum deposition at comparable deposition rates.

A high plasma concentration in the immediate vicinity of the sputtered target owing to the presence of a magnetic field is a distinctive feature of magnetron-sputtering systems. Therefore, in magnetron-sputtering systems, larger negative biases and, consequently, higher sputtering efficiency can be achieved [8].

Features of formation of the structure of deposited coatings will be discussed using the example of a multilayer polycrystalline TiN/TaN coating [9] formed by the magnetron-sputtering method. The purity of the sputtered targets was 99.9% in either case (Ti and Ta). A Ti layer with a thickness of about 20 nm was deposited onto the substrate surface as a transition layer. After that, the coating was formed by alternating deposition of TiN and TaN. The  $l_{\text{TaN}}/l_{\text{TiN}}$  modulation ratio was fixed at 3 : 1. According to X-ray diffraction analysis, the results of which are shown in Fig. 1, single-layer TiN coatings have a cubic structure with a lattice

constant of 0.424 nm and a (200) preferred orientation, while single-layer TaN coatings are characterized by the presence of a cubic phase with a lattice constant of 0.434 nm, a small amount of a hexagonal phase, and the (111) preferred orientation. According to X-ray diffraction patterns of the multilayer TiN/TaN system with different modulation periods, the strongest reflections correspond to the (111), (200), and (311) orientations; this finding confirms the formation of the so-called “superlattice.” With an increase in the modulation period to  $\Lambda = 11.3$  nm, the intensity of the peak corresponding to the (111) orientation significantly increases, while the preferred orientation becomes more pronounced. Along with the change in the modulation period to  $\Lambda = 11.3$ , a hexagonal phase of TaN<sub>0.8</sub> is formed in the coatings. Nordin and Ericson observed a similar phenomenon while studying the features of formation of multilayer TiN/TaN<sub>x</sub> coatings by PVD methods [10].

The use of reactive magnetron sputtering for the preparation of multilayer nitride coatings using the example of Ta/TaN systems was shown in [11], the authors of which studied the tribotechnical characteristics of Ta/TaN coatings formed both by reactive magnetron sputtering and by this method combined with ion implantation. The structure and properties of the deposited coatings were compared with those of a single-layer TaN coating. Figure 2 shows the results of scanning electron microscopy for a multilayer Ta/TaN coating deposited without (Fig. 2b) and with (Fig. 2a) the use of ion implantation. The light and dark layers correspond to Ta and TaN, respectively. Figure 2 clearly shows the alternate structure of Ta and TaN with three modulation periods. Although the total time of preparation of the multilayer Ta and TaN coatings was the same, it was found that the thickness of the sample deposited with the use of ion implantation was lower than the thickness of the coating formed entirely by reactive magnetron deposition. The thickness of the samples was 958.5 nm and 1.167  $\mu\text{m}$ , respectively. This fact can be attributed to fairly high ion energies, which make the sputtering of Ta and TaN layers predominate over the magnetron deposition process.

X-ray diffraction patterns of the single-layer TaN coating and the multilayer Ta/TaN coating are shown in Fig. 3. The diffraction pattern exhibits, in addition to the diffraction reflections of the substrate (marked in the figure as Fe), the basic plane reflections of the cubic lattice of Ta and the hexagonal lattice of TaN. The (110) reflection of the Ta phase exhibited at angles of 37.5° is present in the sample of the multilayer coating. In the single-layer coating, the (110) peak is significantly weaker because of the TaN(110) plane reflection. The hexagonal TaN(001), TaN(110), and TaN(300) reflections are shown as 32, 35, and 62, respectively. The multilayer Ta/TaN sample exhibits a more pronounced TaN(300) peak, a fact that is

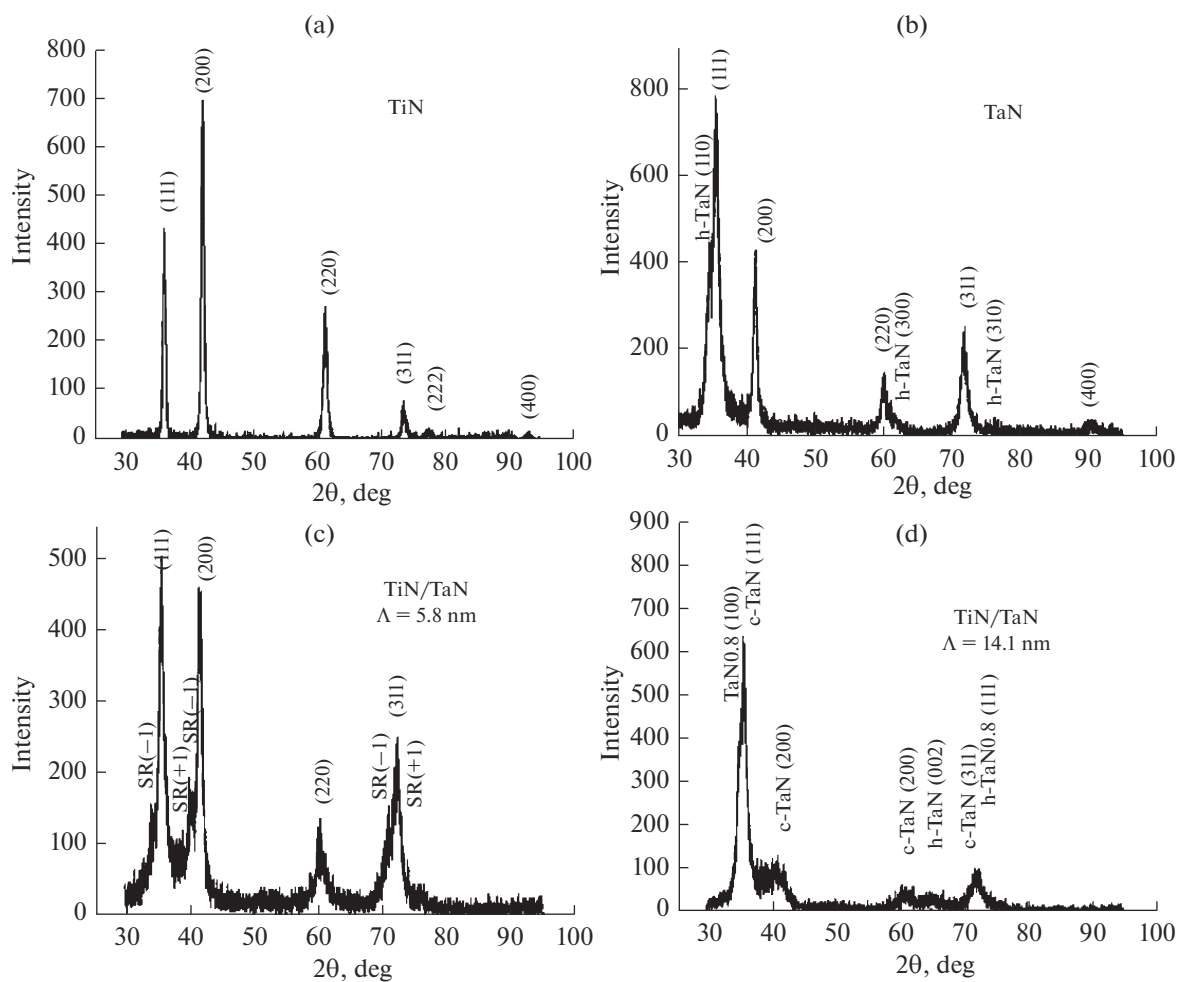


**Fig. 1.** Portions of X-ray diffraction spectra of the single-layer TiN and TaN coatings and the multilayer TiN/TaN coating: (a) TiN, (b) TaN, (c)  $\Lambda = 5.8$  nm, and (d)  $\Lambda = 11.3$  nm [9].

attributed to higher ion energies in the case of reactive magnetron sputtering combined with ion implantation.

The authors of [12–14] describe results of studies of the mechanical properties and thermal stability of Ta-based coatings, which suggest that multilayer coatings based on this element can be potentially used as functional coatings with improved physicochemical characteristics. Ta-based nitride coatings formed by PVD show a variety of complex compounds, particularly bcc  $\alpha$ -Ta(N), hexagonal  $\gamma$ -TaN, hexagonal  $\epsilon$ -TaN,  $Ta_2N$ , WC structure  $\theta$ -TaN, cubic NaCl  $\delta$ -TaN, hexagonal  $Ta_5N_6$ , tetragonal  $Ta_4N_5$ , and orthorhombic  $Ta_3N_5$  phase [15, 16].

Taking into account the increased scientific interest in multilayer nitride coatings based on Ta, the results of [17] are of particular interest. Using magnetron sputtering, the authors of [17] formed a number of nitride coatings with different phase compositions: a-TaN, c-TaN, and a multilayer TaN coating. The coatings were deposited using the Ar gas as a plasma source

and reactive  $N_2$ . The operating pressure was maintained at a level of  $6 \times 10^{-1}$  Pa in a total gas flow of  $20 \text{ cm}^3/\text{min}$ . The Ar/ $N_2$  flow ratio was controlled to provide the proportion of 18/2 and 12/8 to prepare TaN coatings with different compositions and microstructures. The multilayer TaN coating was obtained by sequential deposition of c-TaN (Ar/ $N_2 = 18/2$ ) and a-TaN layers (Ar/ $N_2 = 12/8$ ) to form a 20-nm-thick bilayer. The total coating thickness was about  $1 \mu\text{m}$ . To gain a deeper insight in the structure and phase composition of the deposited coatings, TEM analysis of a-TaN, c-TaN, and the multilayer TaN coating was conducted. Figures 4a and 4d show that the single-layer c-TaN coating is the entire crystalline fcc  $\delta$ -TaN phase with the (111), (200), (220), and (311) preferred orientations. The micrograph (Fig. 4a) clearly shows that c-TaN has a columnar structure, unlike a-TaN, which has an amorphous microstructure with partial inclusions of crystalline TaN (Figs. 4b, 4e). During the deposition of a multilayer a-TaN/c-TaN structure, the

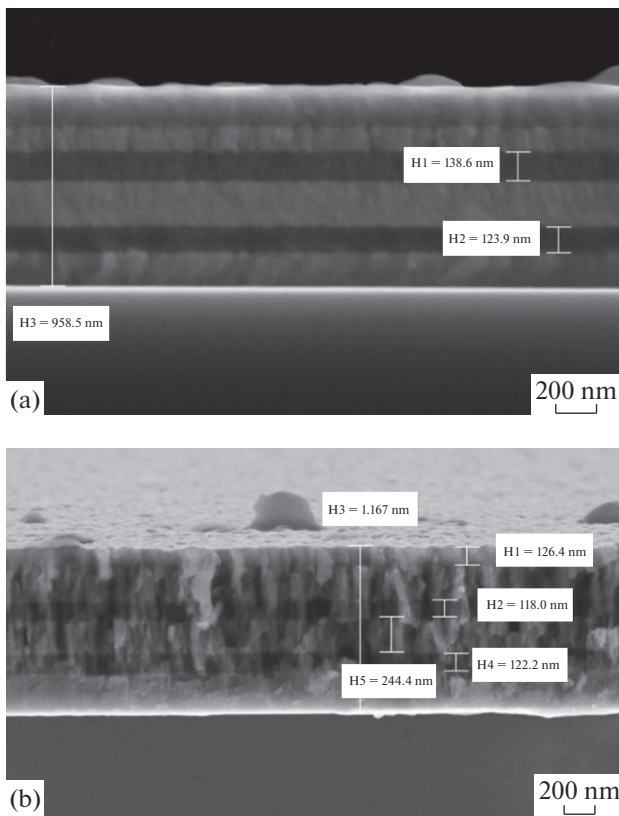


**Fig. 2.** SEM image of the multilayer Ta/TaN coating: (a) with and (b) without ion implantation [11].

space formed in the a-TaN layers is insufficient for the formation of a long range of the crystalline TaN phase.

The dominant effect of the heterostructure configuration of the coating and the thickness of the resulting bilayer on the microstructure and tribological properties will be considered using the example of a CrN/ZrN coating [18]. The multilayer CrN/ZrN coating was deposited by DC magnetron sputtering; in addition, reference samples of single-layered nitride coatings CrN and ZrN were prepared. The base pressure was maintained at a level of  $5.0 \times 10^{-4}$  Pa, and the total working pressure of Ar + N<sub>2</sub> was  $1.5 \times 10^{-1}$  Pa. The periodic structure of the multilayer CrN/ZrN coating was formed by alternating sputtering of Cr and Zr targets for 60 min. In this case, the absence of a transition (adhesive) layer between the coating and the substrate is noteworthy. CrN was deposited as the first layer adjacent to the substrate and the last surface layer.

According to Fig. 5, the single-layer CrN coating is characterized by a B1-type structure with the most pronounced diffraction reflection (200), medium-intensity reflection (111), and weak diffraction reflection (220). The intensity of the ZrN peaks indicates the (111) preferred plane orientation and a weak (222) reflection. The multilayered CrN/ZrN coating has a

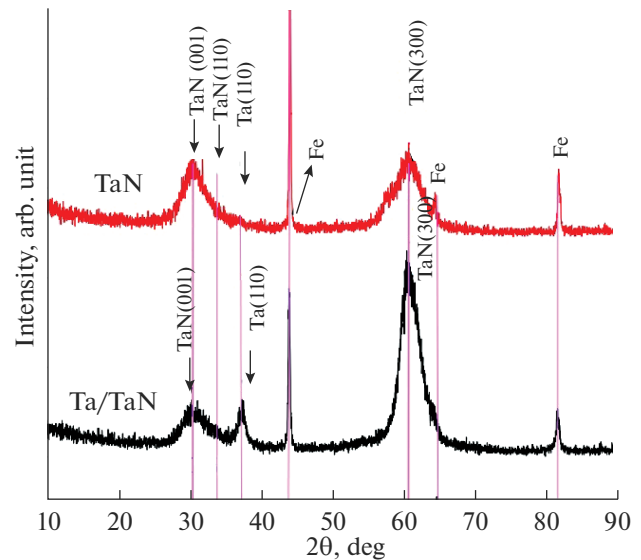


**Fig. 3.** Portions of X-ray diffraction spectra of the single-layer TaN coating and the multilayer Ta/TaN coating.

critical level of internal stresses, as evidenced by intense reflections corresponding to the  $\langle 111 \rangle$  preferred orientation, which tends to minimize the internal stresses [19]. A decrease in the bilayer thickness leads to a constant shift of the CrN reflections toward low angles. The ZrN(111) diffraction peak does not change with a decrease in the bilayer thickness to 35.0 nm. After that, it is shifted toward a higher diffraction angle. At a bilayer thickness of 11.7 nm, the coating is a combination of CrN and ZrN layers with the (111) reflection. These results apparently indicate the formation of a superlattice structure [20].

The authors of [21] prepared a multilayer MoN/CrN coating by vacuum cathodic-arc evaporation. One of the main differences of this method from magnetron sputtering is the higher energy of the sputtered particles. It was a high-priority task for these authors to study the effect of negative bias potential  $-U_b$ , which is responsible for the energy of the deposited particles, and the pressure of the nitrogen atmosphere in the working chamber, which determines the nitrogen content in the coating, on the structural-phase states in the layers of the deposited coatings and their mechanical properties.

The working (nitrogen) atmosphere pressure during deposition was  $P_N = 7 \times 10^{-4} - 3 \times 10^{-4}$  Torr. During deposition, a constant negative potential of  $U_b = -20, -70, -150, \text{ and } -300$  V was applied to the substrates. Figure 6 shows data of analysis of the elemental composition of the coatings as a function of pressure  $P_N$  in the chamber and applied negative potential  $-U_b$ . It is evident that the content of nitrogen, as a light interstitial element, largely depends on the  $P_N$  value during deposition (Fig. 6a). The effect of  $-U_b$  is less

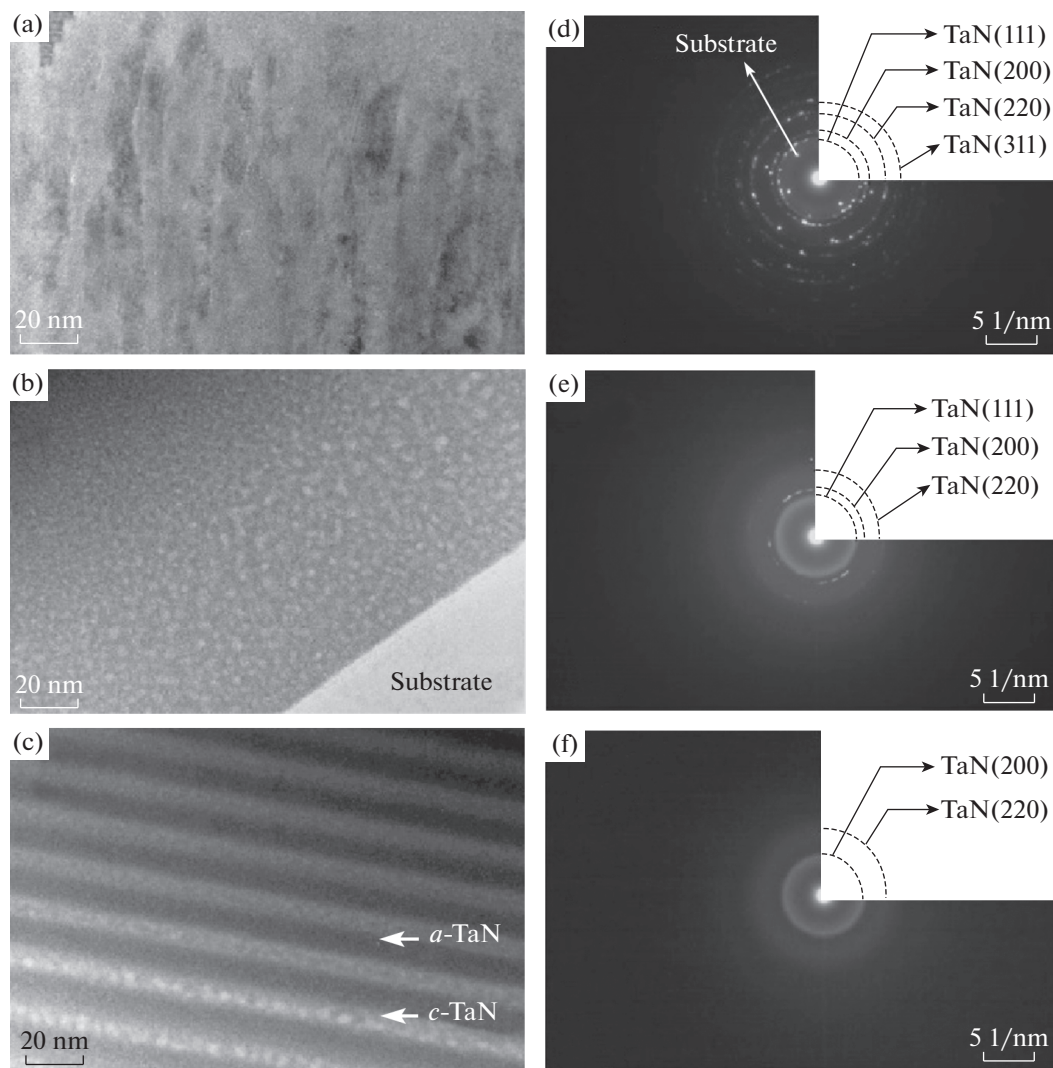


**Fig. 4.** TEM image of the (a) *c*-TaN, (b) *a*-TaN, and (c) Ta/TaN coatings; electron diffraction in individual regions of the (d) *c*-TaN, (e) *a*-TaN, and (f) Ta/TaN coatings [17].

pronounced (Fig. 6b), this being evident as a relative decrease in the atomic nitrogen concentration at large values of bias potential  $-U_b$  (owing to selective secondary sputtering from the growth surface). Note that the strengthening of the bond between the deposited metal and atmospheric nitrogen at high pressure  $P_N$  leads to stabilization in the coating composition to significantly larger  $-U_b$  values (Fig. 6b, curve 2). A considerable difficulty in the coating deposition by vacuum-arc evaporation lies in the fact that, if the cathode spot stays at an evaporation point for too long, it will emit a large number of macroparticles or droplets. These macroinclusions degrade the characteristics of the coatings because they have poor adhesion to the substrate and can emerge through the coating if their size exceeds the coating thickness. Note that another approach to decreasing the droplet component in the

coating is the use of pulsed beams for evaporation [22, 23].

The authors of [24] used the method of vacuum-arc deposition to prepare TiN/ZrN coatings. The resulting biphasic multilayer TiN/ZrN system had a nanometer-range thicknesses and a fairly high planarity. During the experiment, these authors deposited three sets of coating samples with different thicknesses of the bilayer period. The total pressure in the deposition chamber was  $P_N = 3 \times 10^{-3}$  Torr at a bias potential of  $-150$  V. In the first set of samples, the thickness of one bilayer ( $\Lambda$ ) of the TiN/ZrN coatings was about 40 nm at a total coating thickness of about 13  $\mu\text{m}$ . In the second set of samples, the thickness of the TiN/ZrN bilayer period was increased to  $\Lambda \approx 70$  nm at a total coating thickness of  $h \approx 14$   $\mu\text{m}$ . The third set of TiN/ZrN multilayer coatings was deposited with a

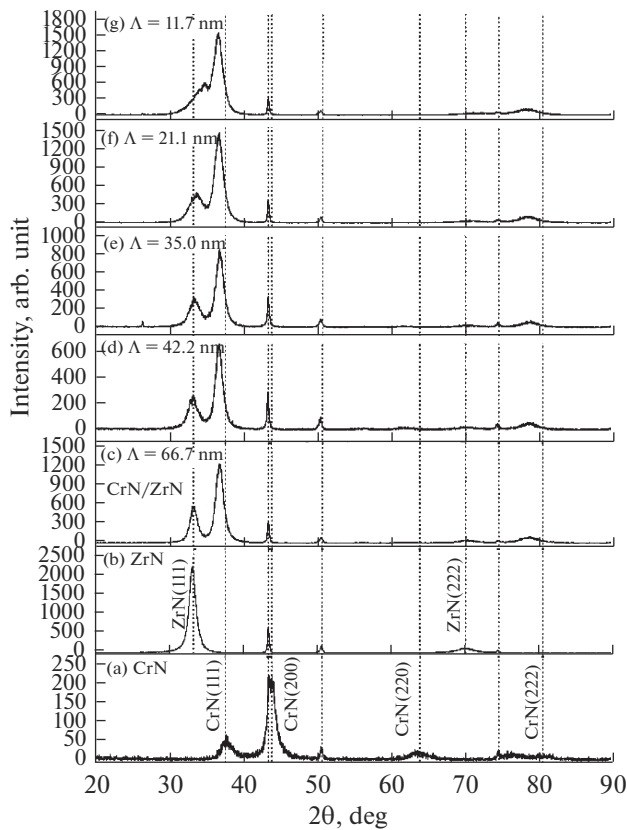


**Fig. 5.** Portions of X-ray diffraction spectra for the CrN and ZrN monolayers and the multilayer CrN/ZrN coating [18].

bilayer-period thickness of  $\Lambda \approx 250$  nm and a total coating thickness of  $h \approx 14$   $\mu\text{m}$ .

Figure 7 shows a fragment of the X-ray diffraction pattern of samples of these multilayer coatings. It is evident that the coating consists of TiN and ZrN phases with a cubic crystal lattice (NaCl structural type) without any preferred orientation (texture). The intensity of the reflection corresponding to the TiN layer slightly increases with increasing bilayer thickness, as evidenced by a change in the ratio of intensities of the TiN and ZrN phase reflections (Figs. 7a, 7b). The lattice period in the layers varies with an increase in the deposition time and the total period of the multilayer system. The nitrides formed during deposition have a preferred orientation of the crystallites with the (111) axis perpendicular to the growth plane of the coating. Hence, the preferred orientation of the TiN and ZrN crystallites with the (111) axis is formed at the initial stage of growth under the action of compressive stresses. In addition, the high packing density of the layers hinders the diffusion of oxygen deep into the coating during thermal exposure. Therefore, the formation of oxides during annealing occurs only in the near-surface layer of the coating (up to 5  $\mu\text{m}$ ).

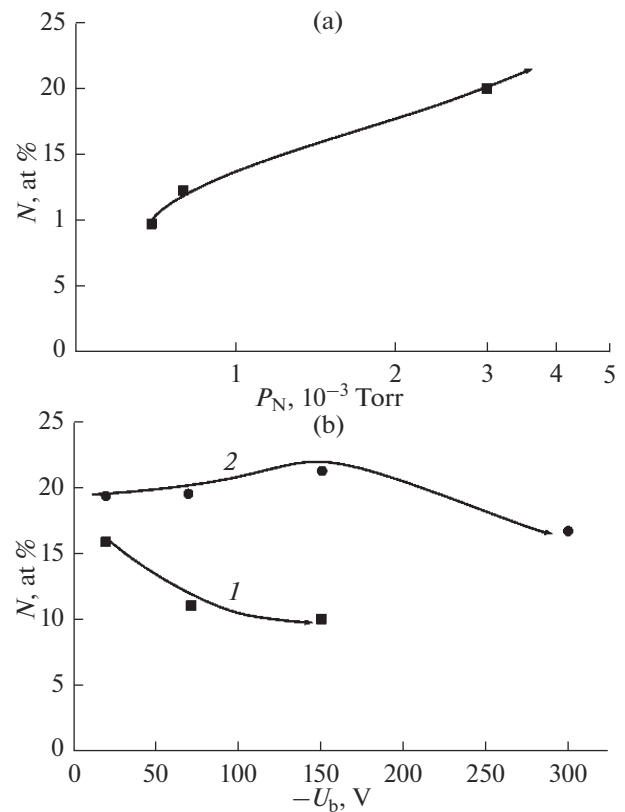


**Fig. 6.** Variation in the nitrogen content in the coating (a) as a function of pressure during deposition ( $P_N$ ) at a constant  $U_b = -70$  V and (b) as a function of  $U_b$  at a constant  $P_N$  of (curve 1)  $7 \times 10^{-4}$  and (curve 2)  $3 \times 10^{-3}$  Torr [21].

The unsatisfactory performance properties of binary nitride coatings (TiN, TaN, VN, etc.) have led to the necessity of doping binary compounds with additional elements, such as Al, Cr, Si, and B, in order to improve the strength and tribological characteristics. Previous studies have shown that the thermal stability of a multicomponent TiAlN coating can be increased by incorporating Cr into it to form chromium nitrides, which exhibit excellent corrosion and wear resistance [25, 26]. A change in the Cr concentration and the thickness of the CrN layers in a multilayer nanocomposite TiAlCrN coating affects the microstructure and mechanical properties of the coating [27, 28].

The authors of [29] prepared TiAlN/CrN cathodic-arc coatings with a thickness of alternating layers of 8 and 17 nm. X-ray diffraction spectra of the multilayer TiAlN/CrN coatings ( $\Lambda = 8$  and 17 nm) are shown in Fig. 8. According to X-ray diffraction analysis, TiAlN/CrN has a B1-NaCl crystal structure with the (111) preferred orientation. The positions of the reflections are the averaged position of the reflections of the TiAlN and CrN phases. The (200) diffraction reflection is asymmetric owing to the presence of TiAlN and CrN phases (inset in Fig. 8). It was found

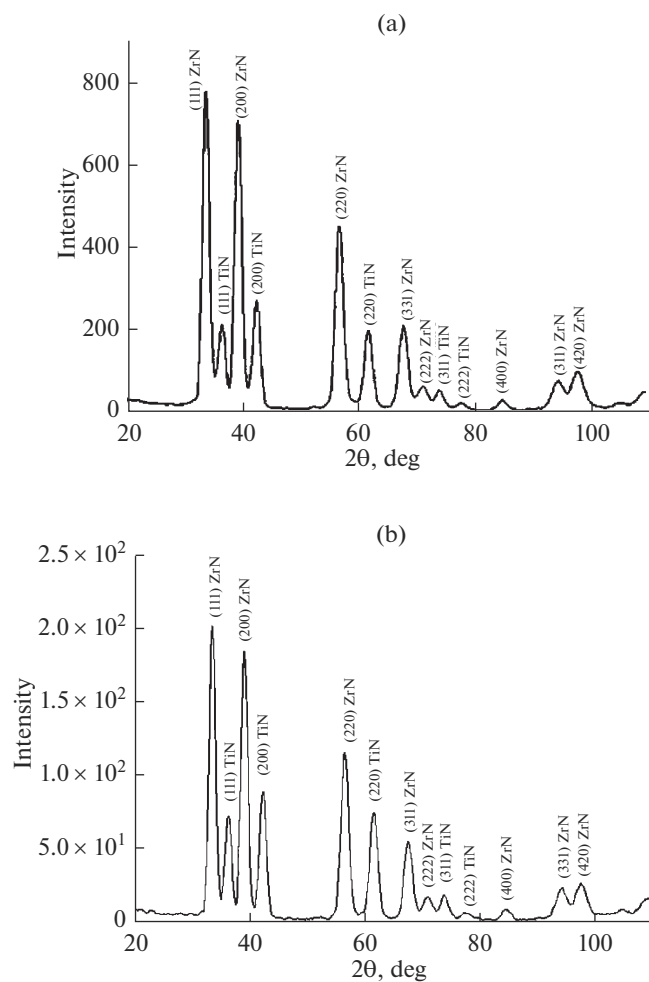


**Fig. 7.** Portions of X-ray diffraction spectra of the multi-layer TiN/ZrN coating at different thicknesses of the bilayer period ( $\Lambda$ ):  $\Lambda \approx$  (a) 70 and (b) 250 nm [24].

that CrN has a higher intensity in the averaged (200) plane reflection in the multilayer TiAlN/CrN coating with an alternating-layer thickness of 8 nm. This finding suggests that the CrN layers will affect the development of the  $\langle 200 \rangle$  texture in multilayer TiAlN/CrN systems deposited with different thicknesses of alternating layers. In addition, a change in the width of the layers will lead to a competitive growth of the CrN and TiAlN phases in the multilayer TiAlN/CrN coating.

Micrographs of the cross section of the TiAlN/CrN cathodic-arc coatings ( $\Lambda = 8$  and 17 nm) are shown in Fig. 9. The coatings have a dense columnar structure. However, the occurrence of ion-induced processes leads to the accumulation of point defects and small dislocation loops, which causes a continuous renucleation of new grains during growth and, as a consequence, a violation of the columnar structure of the coating. The micrographs of the TiAlN/CrN cross sections show the difference between the TiAlN and CrN layers. The CrN layers

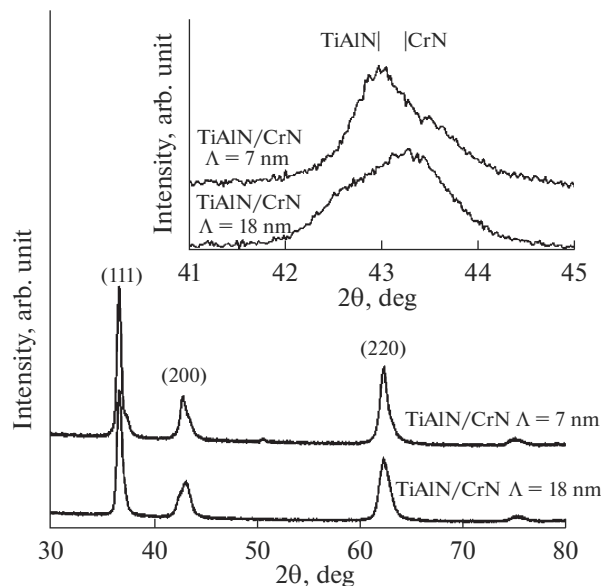


**Fig. 8.** Portions of X-ray diffraction spectra of the multi-layer TiAlN/CrN coatings with the thickness of alternating layers of  $\Lambda = 7$  and 18 nm.

have a brighter contrast because they reflect a larger number of electrons. For both types of TiAlN/CrN systems with  $\Lambda = 8$  and 17 nm, CrN was deposited as a transition layer between the substrate and the coating. The most pronounced layered structure is observed for the TiAlN/CrN coatings with the larger layer thickness ( $\Lambda = 17$  nm); the TiAlN/CrN layer interfaces at  $\Lambda = 8$  nm have fuzzy contours owing to the occurrence of interlayer diffusion.

The multilayered architecture of functional coatings makes it possible to affect the crystallite size and thereby change their mechanical characteristics. Crystallite sizes and lattice deformations for TiAlN/CrN were calculated in accordance with the Williamson–Hall plot. Compared with single-layer TiAlN and CrN coatings, the crystallite size in the multilayer coating decreased by 11 nm to a value of 31 and 38 nm for TiAlN/CrN with  $\Lambda = 17$  and 8 nm, respectively. The decrease in the grain size is attributed to the formation of interfaces between the layers [30]. The grain sizes in the multilayer coating with the smaller layer thickness should have a proportionally smaller grain size. The increase in the crystallite size of TiAlN/CrN with  $\Lambda = 8$  nm is most probably attributed to the diffusion of atoms between the layers during cathodic-arc deposition.

Depending on the energy conditions of deposition, the coatings can be in amorphous and nanocrystalline states and in a nanocrystalline state with a predominantly oriented (columnar) structure. Nitride coatings based on an extended group of refractory metals exhibit a tendency to forming two preferred growth directions, namely, with the (111) or (200) plane. The

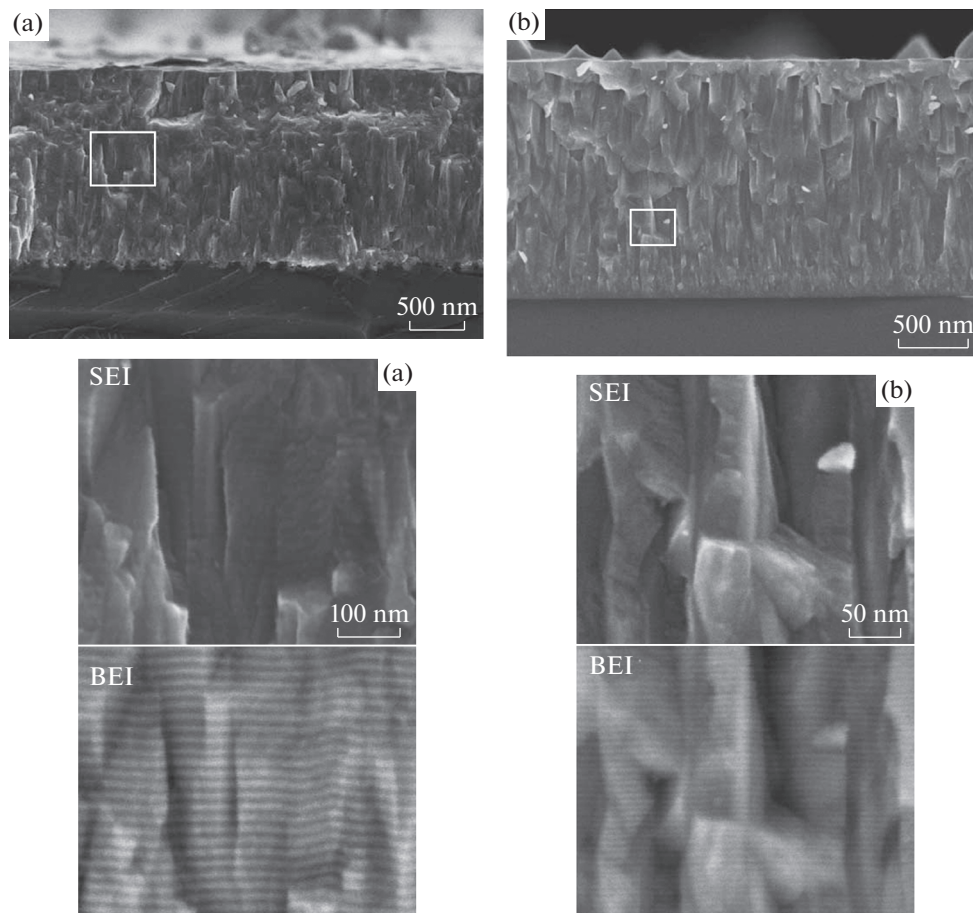


**Fig. 9.** SEM image of the cross section of multilayer TiAlN/CrN coatings with a thickness of alternating layers of  $\Lambda =$  (a) 18 and (b) 7 nm.

(111) plane is a plane of the densest packing for the NaCl structure, while the (200) plane is the most open direction for channeling [31]. A significant difference in the formation of the growth texture is observed in the Ta-based single-layer and multilayer systems discussed in this review. During the synthesis of TaN and Ta/TaN coatings, preferred growth of the (001), (110), (300), and (311) planes is observed.

Quite recently, the notion of multicomponent HEAs has been proposed to increase the thermal stability of nanomaterials. According to this thesis, which has been proven by experiments for various HEAs [32–35], a high entropy of mixing can stabilize the formation of a disordered solid-solution phase and prevent the formation of intermetallic phases during crystallization. HEAs formed in this way can simultaneously exhibit high strength and a fairly high ductility. HEA nitrides exhibit even better mechanical and tribological properties [36–40]. However, these materials are characterized by a significantly higher fragility and lower strength. In this case, the functional properties can be effectively improved via switching to multi-

layer composites with alternating layers of nitrides with different compositions [41–43].

The authors of [44] deposited layers of nitrides of Ti–Zr–Nb–Ta–Hf HEAs and group VI transition metals (W or Mo). Multilayer (TiZrNbTaHf + W)N and (TiZrNbTaHf + Mo)N coatings were prepared by vacuum-arc deposition while varying the negative bias potential across the substrate  $U_b$  from –90 to –280 V.

Studies of the morphology of growth of the multilayer coatings showed a fairly high homogeneity and planarity of the deposited layers in all the used modes for both types of systems (TiZrNbTaHf + Mo)N and (TiZrNbTaHf + W)N. The partial presence of inhomogeneities in the form of droplet fractions on the surface did not lead to a significant violation of the planarity and average thickness of the deposited coatings.

The bias potential and the working nitrogen-atmosphere pressure had a decisive effect on the phase composition and structural state of the coatings. Figure 10 shows portions of the X-ray diffraction spectra of coatings deposited under different technological conditions. Analysis of the diffraction spectra shows that all deposition modes are characterized by the for-



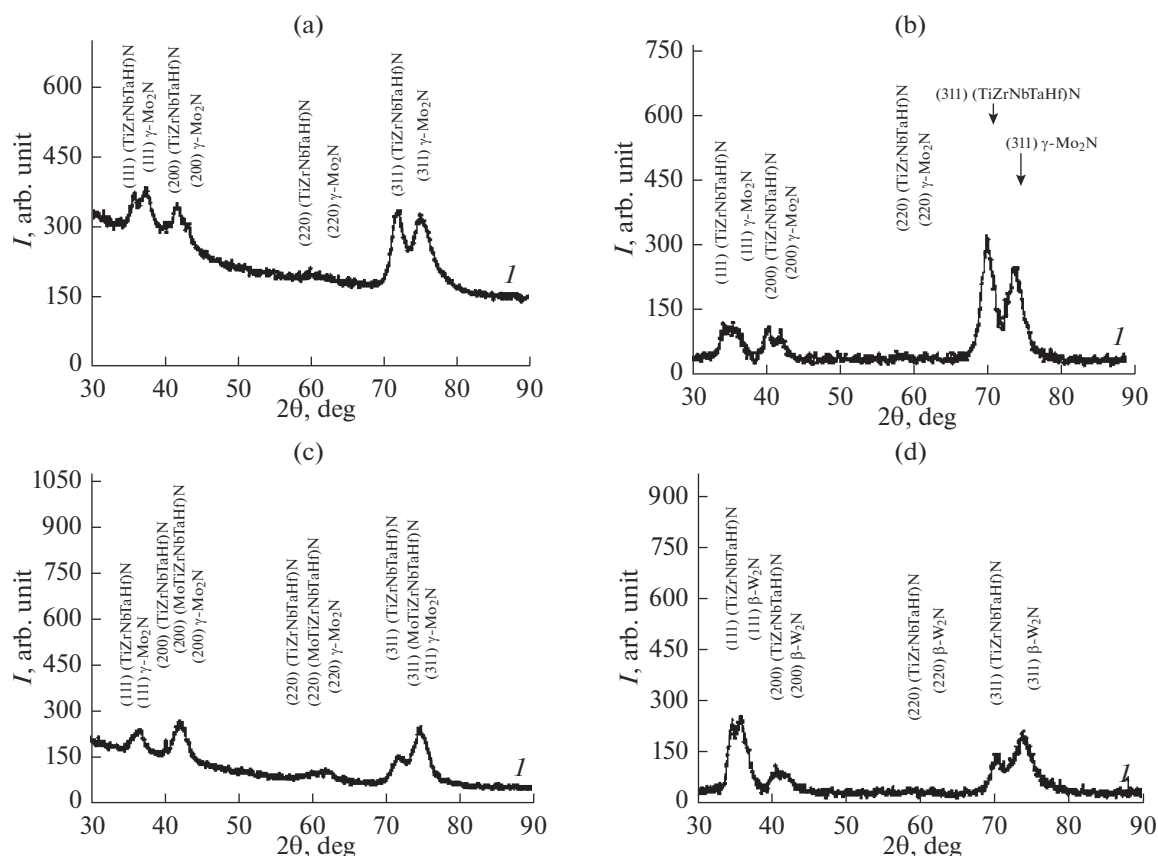


**Fig. 10.** Portions of X-ray diffraction spectra of the (TiZrNbTaHf)N/MoN coating at (a)  $P_N = 1.5 \times 10^{-3}$  Torr,  $U_b = -50$  V; (b)  $P_N = 4 \times 10^{-3}$  Torr,  $U_b = -50$  V; and (c)  $P_N = 4 \times 10^{-3}$  Torr,  $U_b = -200$  V, and (d) the (TiZrNbTaHf)N/WN coating at  $P_N = 4 \times 10^{-3}$  Torr,  $U_b = -90$  V [44].

mation of phases with a cubic (fcc) crystal lattice in all layers of the multilayer coatings. In HEA-based layers, it is an unordered solid solution of (TiZrNbTaHf)N with a crystal lattice of the NaCl structural type [45]; in the layers of the Mo–N system, it is the  $\gamma$ -Mo<sub>2</sub>N phase; and, in the layers of the W–N system, it is  $\beta$ -W<sub>2</sub>N (PDF 25-1257). The similarity of structural states in the layers based on HEAs and nitrides of group VI transition metals (close ratio of the formed preferred orientations of crystallites in the layers) suggests that there is a relationship between the structure of the layers and their growth.

These spectra also show that an increase in the working nitrogen-atmosphere pressure leads to an increase in the degree of texturing, as evidenced by a relative increase in the intensity of the reflections. Thus, at relatively low  $U_b$  values in the (TiZrNbTaHf)N/MoN coatings, this texture has the (311) axis (Figs. 10a, 10b). The application of a high negative bias potential of  $U_b = -200$  V leads to an increase in the degree of “chaotization” of the structure (the texture characteristic of low  $U_b$  values does not appear at high  $U_b$  values) and to an increase in the degree of dispersion of crystalline entities in the coating layers,

which is most pronounced for the  $\gamma$ -Mo<sub>2</sub>N layers (Fig. 10d).

The preferred direction of growth of multicomponent and highly entropic nitride coatings is determined by the complex mechanism of interaction of “kinetic” effects associated with the growth process [31].

#### TRIBOLOGICAL PROPERTIES OF MULTILAYER COATINGS BASED ON REFRACTORY METALS

Many reports describing the results of tribological tests of single- and multilayer coatings based on refractory metal nitrides have been published [46–49]. The keen interest in functional coatings of this kind is mostly due to the extensive range of their potential application. In the aerospace, automotive, and military industries, the requirements for parts, assemblies, and entire mechanisms operating under dry friction conditions, at high temperatures, and under the action of an aggressive environment are being constantly tightened. Multilayer nitride systems have been effectively used in the manufacture of driveline compo-

**Table 1.** Mechanical and tribological characteristics of Ta-based coatings [11]

	Hardness, GPa	Coefficient of friction	Volume of worn material, $\mu\text{m}^3$
Substrate (Cr12MoV)	4.44	0.6	48.9
TaN	9.02	0.2–0.4	29.6
Ta/TaN	12.93	0.1–0.25	14.3
Ta/TaN*	10.92	0.1–0.25	19.4

\* The coating was deposited with the use of ion implantation.

nents, cutting tools, helicopter gearboxes and blades, compressor blades of engines with a high thrust-to-power ratio, and other mechanisms operating under high load conditions. In this context, it is necessary to increase the servicing period and the level of reliability and improve the tribotechnical characteristics of the used coatings.

Properties of multilayer coatings are determined by their structure and element composition; which is a key parameter that affects the tribological properties is the modulation period of layers in a multilayer system. Below, the most interesting and striking—according to our reckoning—results of many tribological and tribotechnical tests of multilayer coatings are discussed. Results of comparative tribological tests of a multilayer TiN/TaN coating and a single-layer TiN coating are reported in [9]. The measurement of the coefficient of friction can be conventionally divided into two stages: an initial (lapping) stage and a stable stage. The lowest coefficient of friction is observed at the beginning of measurements; after that, the coefficient gradually increases to some stable values. The establishment of a stable stage for the friction values took longer time for the multilayer TiN/TaN coating, a finding that is apparently attributed to the fact that the hardness of this coating is higher than that of the single-layer TiN coating. The coefficient of friction of the TiN/TaN coatings was 0.7–1.0 as opposed to 0.5 for the single-layer TiN coating. At the same time, an inverse relationship between a decrease in the volume of the worn material and an increase in the coefficient of friction is observed.

To determine the wear mechanisms of the multilayer TiN/TaN system, the authors analyzed the morphology of coating samples with different modulation periods (Fig. 11). It should be noted that the wear track mostly consists of grooves; the wear-track width decreases with increasing hardness of the multilayer coating. During the tribological tests, a small amount of the material is transferred from the wear-track grooves, as evidenced by Figs. 11a and 11b and the respective energy-dispersive X-ray spectroscopy (EDX) analysis. The formation of cleavages and the transfer of the material to the wear track surface can be associated with high compressive stresses within the coating. Poor adhesion to the substrate caused by high

compressive stresses is characteristic of TiN/TaN coatings with a modulation period of about 10 nm, which has also been mentioned by other authors [3]. As the modulation period increases, the pattern of wear of the track surface becomes smoother (Figs. 11c, 11d). Thus, despite the fact that the coefficient of friction of the single-layer TiN coating is lower than that of the multilayer TiN/TaN coating, the wear resistance of the latter is significantly higher.

Particular attention should be paid to [11], in which tribological and industrial tribotechnical tests of Ta-based nitride coatings are described. Table 1 shows results of mechanical and tribological tests for three types of Ta-based coatings. The multilayer Ta/TaN coating has the highest hardness, the lowest coefficient of friction, and the best wear resistance of the three test samples. It can be assumed that the relatively low hardness of the multilayer Ta/TaN coating prepared with the use of ion implantation is a natural result of the intense ion bombardment of the surface because implantation with heavy ions leads to the disintegration (crushing) of the nanograins and the formation of a disordered polycrystalline structure without any preferred orientation [50, 51].

For tribotechnical tests, the authors of [11] covered the parts of a fuel-injection pump with a multilayer Ta/TaN system. It was deposited with and without ion implantation. The aim of this experiment was to extend the lifetime of the aircraft-engine parts. Figure 12a shows a fuel-injection pump part with a multilayer Ta/TaN coating after 1500 h of operation. A partial delamination of the functional coating is observed in contrast to the part shown in Fig. 12b. Owing to the multilayer Ta/TaN system formed with the use of ion implantation, the failure-free operation time of the pump part increased by five times. In this context, it can be assumed that the alternation of ion implantation and deposition makes it possible to remove residual stresses and increase the ductility of the material, which in turn improves the adhesion of the coating to the material of the part.

The effect of modulation period of bilayers  $\Lambda$  on the tribological characteristics of a multilayer CrN/ZrN coating was studied in [18]. For tribological tests, two samples of a multilayer CrN/ZrN coating ( $\Lambda = 66.7$  and 11.7 nm) were prepared. As in the case of

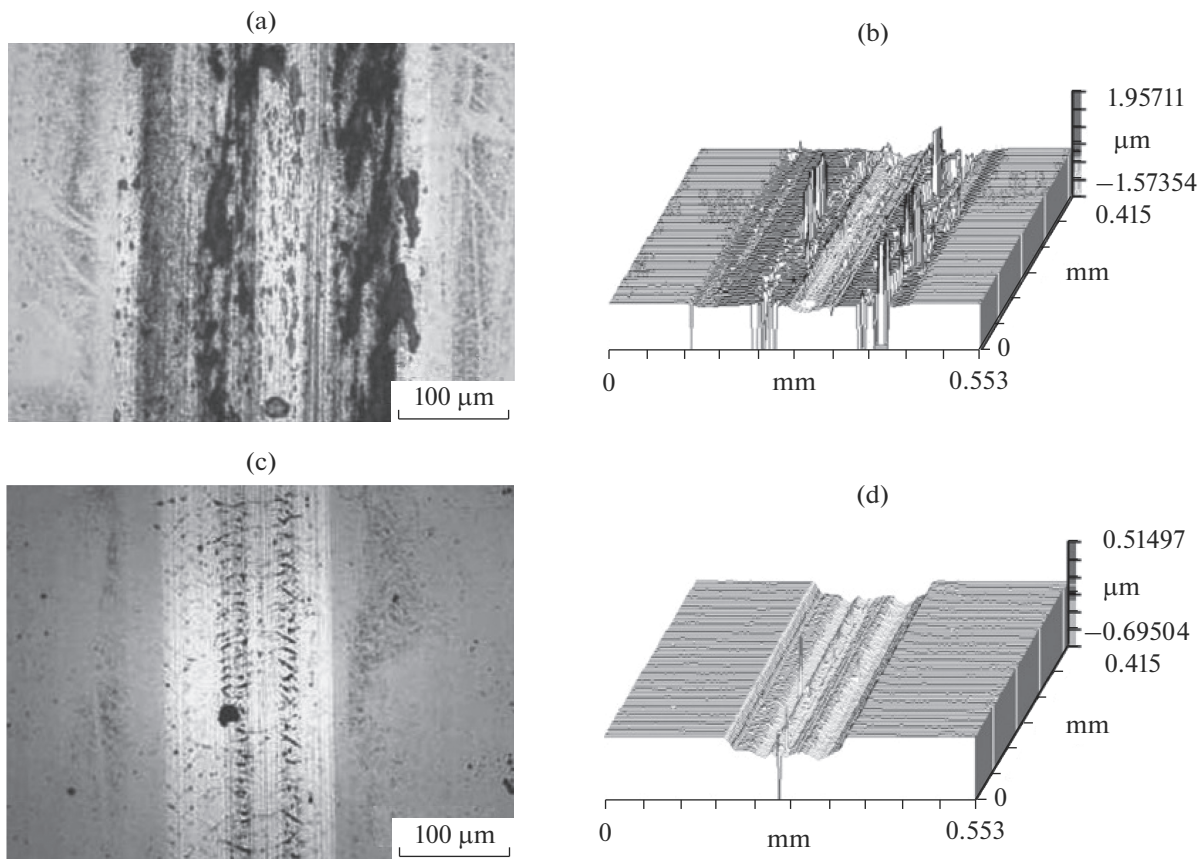


**Fig. 11.** Optical micrographs and the corresponding 3D images of the wear tracks of the multilayer TiN/TaN coating with different modulation periods: (a, b) 2.8 and (c, d) 8.5 nm [9].

other multilayer systems, the measurement of the coefficient of friction can be conventionally divided into two stages: an initial (lapping) stage and a stationary mode. An abrupt increase in the coefficient of friction at the initial stage can be caused by the action of oxide layers formed on the coating surface and a change in the contact stresses. The coefficient of friction and the volume of the worn material increase with decreasing modulation period  $\Lambda$ . For the multilayer CrN/ZrN system with  $\Lambda = 66.7$ , the coefficient of friction was 0.32 and the volume of the worn material was  $1 \times 10^{-7} \text{ mm}^3/\text{m}$ , while for CrN/ZrN with  $\Lambda = 11.7$ , the coefficient of friction and wear volume increased to 0.54 and  $5.5 \times 10^{-7} \text{ mm}^3/\text{m}$ , respectively. For a more detailed analysis of the morphology of the coatings, the authors constructed a 3D model of the sample surface after tribological tests (Figs. 13c, 13d).

Figure 13a clearly shows a valley (formation of a groove) in the middle of the wear track. According to Fig. 13c, there is a large amount of the accumulated (transferred) material around the wear track. EDX analysis revealed that the accumulated material contain W from the surface of the counterbody. The high temperature resulting from dry friction led to the pressing of the counterbody particles into the coating

surface and the formation of oxides; it is this process that affected the coefficient of friction.

Figure 13b shows a broader wear track and a uniform cohesive pattern of wear of the material. The authors of [18] assert that the strong wear suggests that this coating is a more effective barrier preventing cutting-tool degradation caused by plastic deformation or the formation of microcracks.

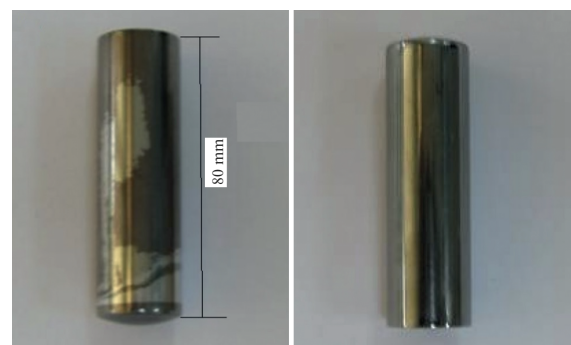


**Fig. 12.** Photographs of fuel-pump parts: (a) the multilayer Ta/TaN coating and (b) the multilayer Ta/TaN coating deposited with the use of ion implantation [11].

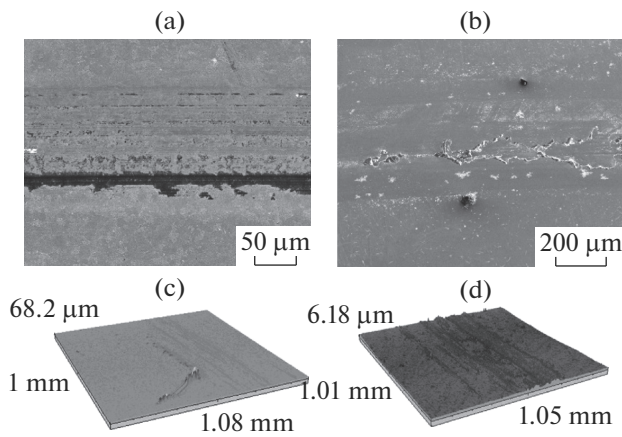


**Fig. 13.** Micrographs of the surface and 3D images of the multilayer CrN/ZrN coating after the tribological test:  $\Lambda =$  (a, c) 66.7 and (b, d) 11.7 nm [18].

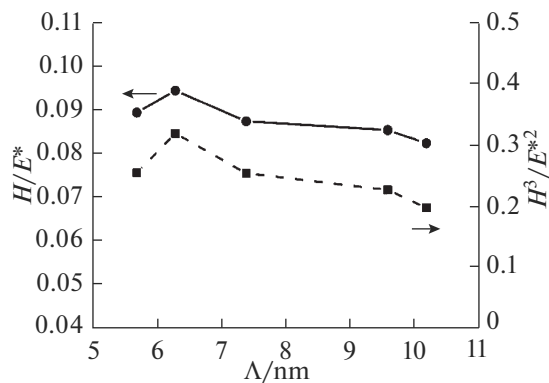


**Fig. 14.** Graphical representation of the results of calculation of the  $H/E^*$  and  $H^3/E^{*2}$  ratios as a function of modulation period  $\Lambda$  in the multilayer CrN/TiN coating [52].

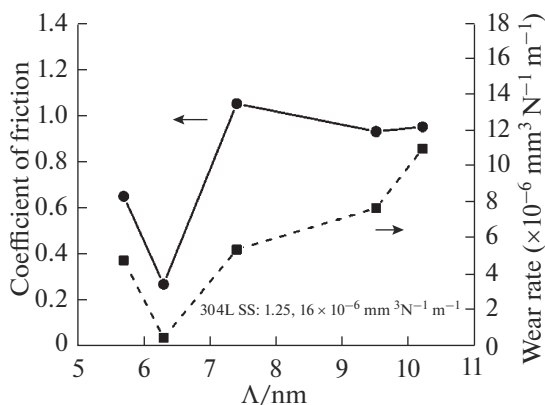


**Fig. 15.** Results of measurements of the coefficient of friction and wear rate of the multilayer CrN/TiN coating as a function of modulation period  $\Lambda$  [52].

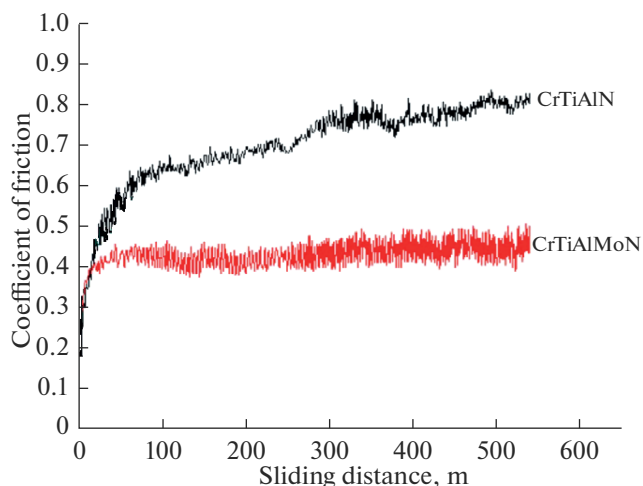
The effect of structural features and mechanical characteristics on the tribological properties of a multilayer CrN/TiN system was studied in [52]. In accordance with the theory of wear of materials, hardness is considered one of the indirect parameters of increase in wear resistance [53]. However, despite high hardness, a number of functional coatings are characterized by low plastic strains and proneness to severe surface cracking [54]. In this context, the authors of [54] analyzed the elastic and plastic strains ( $H/E^*$  and  $H^3/E^{*2}$ ) and their effect on the tribological properties, wear mechanism, and adhesion strength of a multilayer CrN/TiN coating.

Figure 14 shows results of calculations of  $H/E^*$  and  $H^3/E^{*2}$  for a set of multilayer CrN/TiN coatings with a modulation period of  $\Lambda = 5.7\text{--}10.2$  nm. At  $\Lambda = 5.7\text{--}10.2$  nm, the  $H/E^*$  and  $H^3/E^{*2}$  ratios increased from 0.089 to 0.094 and from 0.222 to 0.316 and then decreased to 0.082 and 0.195, respectively. An increase in the  $H/E^*$  and  $H^3/E^{*2}$  ratios is achieved owing to a decrease in the modulation period of the bilayer to  $\Lambda = 6.3$  nm.

Results of tribological tests of a set of multilayer CrN/TiN coatings are shown in Fig. 15. The dependence of the coefficient of friction and the volume of the worn material on modulation period  $\Lambda$  was studied by the ball-on-disc method. It should be noted that coatings with high  $H/E^*$  and  $H^3/E^{*2}$  values and the optimum period  $\Lambda$  ( $\Lambda = 6.3$  nm) have the densest structure and the highest impact strength [14, 17, 55–58]. An increase in  $\Lambda$  led to a decrease in the density and number of interfaces and to an increase in the grain size, which correlates with a decrease in the  $H/E^*$  and  $H^3/E^{*2}$  ratios. An abrupt increase in the coefficients of friction at  $\Lambda = 9.5\text{--}10.2$  nm is caused by the formation of oxides in the near-surface area of the coatings, while the subsequent increase in the wear intensity is attributed to the continuous delamination of the coating. Vigorous delamination of the coating layers and deterioration of adhesion to the substrate resulted from the presence of high residual stresses, which arose from an increase in the power applied to the Cr target, an increase in  $\Lambda$ , and an increase in the total coating thickness.

#### *Mechanical and Tribological Properties of Multilayer Coatings with an Adaptive Friction Mechanism*

In the context of this review, it is important to discuss the class of functional coatings with an adaptive friction mechanism [59–62, 101]. A specific feature of adaptive coatings is the ability to change their properties—primarily, the coefficient of friction—depending on the operating conditions. The mechanical and tribological properties of adaptive coatings will be analyzed using the example of a multilayer CrTiAlMoN system [63]. It is known that nanocomposite CrTiAlN coatings exhibit a fairly low wear rate, a high oxidation



**Fig. 16.** Results of measurements of the coefficient of friction by the ball-on-disc method [63].

resistance, and a fairly high temperature stability; therefore, CrTiAlN can be effectively used, for example, for dry cutting [64]. According to the literature, at high temperatures, MoN can form oxygen-deficient phases (Magnéli phases) and has a low coefficient of friction [65, 66]. However, a binary MoN coating is not suitable for practical applications because it is highly oxidizable. A combination of CrTiAlN and MoN into a multilayer CrTiAlMoN system provides the formation of an adaptive functional coating with improved mechanical and tribological characteristics.

Figure 16 shows results of measurements of the coefficient of friction for the CrTiAlN and CrTiAlMoN coatings. According to expectations, the multilayer CrTiAlMoN system exhibits a significantly lower coefficient of friction (0.43) than that of CrTiAlN (0.78). This substantial decrease in the coefficients of friction is apparently due to the fact that Cr, Ti, and Al have different effects on the formation of molybdenum oxide and the occurrence of the lubrication effect during friction. A considerable effect of Al on the formation of an oxide film and a significant decrease in the coefficients of friction of molybdenum-containing coatings were confirmed in [67].

Optical micrographs of the wear tracks of CrTiAlN and CrTiAlMoN are shown in Fig. 17. It is evident from the micrographs that the width of the wear track of CrTiAlMoN is much smaller than the corresponding parameter of CrTiAlN; in this case, there is hardly any accumulation of the worn material along the edges of the wear track. Visual inspection of the worn (transferred) material (Figs. 17a, 17b) suggests that the coating underwent abrasive wear during a ball-on-disc test. EDX studies of the wear products of the two coatings showed the presence of the W element only in the spectrum of CrTiAlN, a finding that suggests that a significant amount of the material was transferred

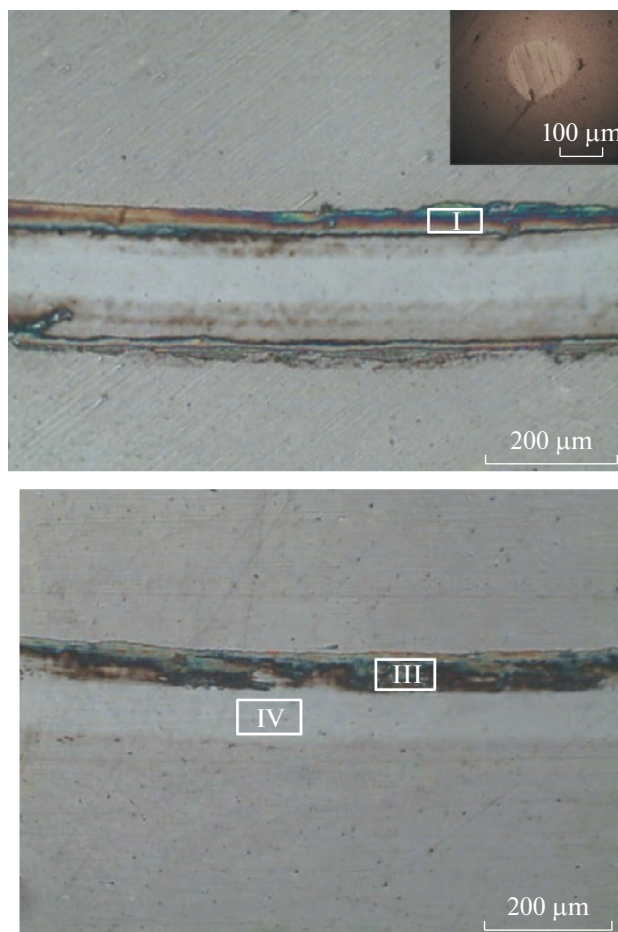


**Fig. 17.** Optical micrographs of the coating surface after tribological tests by the ball-on-disc method: (a) CrTiAlN and (b) CrTiAlMoN [63].

from the counterbody (WC–Co) to the coating surface. A similar effect of the transfer of the counterbody material is described in [18]. Elemental analysis of the CrTiAlMoN coatings revealed almost complete absence of oxygen on the surface of the wear track and the presence of molybdenum oxide in the worn material. Hence, the incorporation of Mo into the composition of nitride coatings based on refractory and transition metals contributes to a decrease in the coefficient of friction during the formation of an oxide (lubricating) film.

The authors of [68] developed an adaptive CrN/VN coating as a product for tribotechnical purposes. During the experiment, sets of multilayer CrN/VN systems with a variable modulation period ( $\Lambda = 7, 13, \text{ and } 27 \text{ nm}$ ) were deposited to study the effect of the multilayer structure on the hardness and tribological characteristics of the deposited coatings. Results of tribological tests for multilayer CrN/VN and single-layer CrN and VN coatings are shown in Fig. 18. The coefficients of friction of the multilayer coatings are lower than the coefficients of the single-

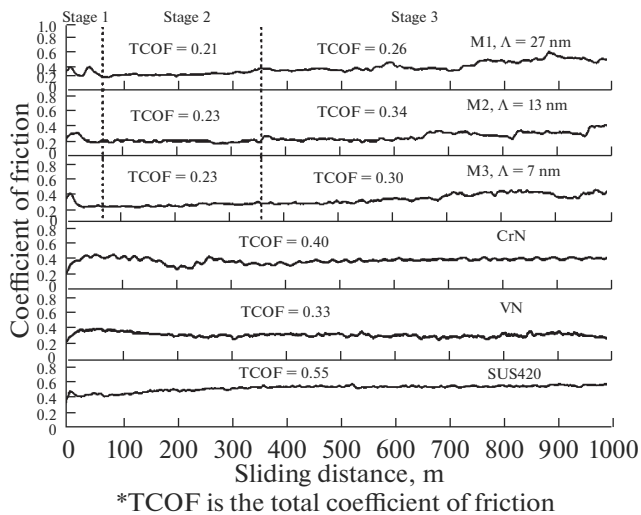


**Fig. 18.** Results of measurements of the coefficient of friction for the CrN and ZrN monolayers and the multilayer CrN/VN coating [68].

layer (reference) samples; this finding suggests that the use of a multilayer system is more advantageous. The measurement of the coefficient of friction for CrN/VN can be divided into three stages. Stable values of the coefficient of friction correspond to the second stage of measurements, because, at the initial stage, an increase in the studied parameter is the result of changes in the contact stresses and the effect of surface roughness. Thus, the coefficient of friction of the CrN/VN coatings was 0.21 at  $\Lambda = 27$  nm and 0.23 at  $\Lambda = 7$  and 13 nm. According to Lu et al. [69], during a ball-on-disc test,  $H_2O$  will react with the worn material to form metal oxides. The presence of vanadium oxides, particularly  $V_2O_3$  and  $V_2O_5$ , in the worn material is confirmed by analysis of the  $V 2p_{3/2}$  XPS spectra (Fig. 19). A decrease in the coefficient of friction of the multilayer CrN/VN coating is caused by the reaction of VN with water and, as a consequence, the formation of vanadium oxide, which plays the role of a lubricant [70]. An increase in the coefficients of friction at the third stage is attributed to the effect of an SUS 420 substrate, severe wear, and a decrease in the coating thickness.

### THERMAL STABILITY AND CORROSION RESISTANCE OF MULTILAYER NITRIDE COATINGS

Materials that preserve their original structure and properties under the effect of high temperatures are conventionally referred to as “thermally stable (heat-resistant) materials” [71–76]. In the context of this review, the studied temperature range is up to 1100°C. An exposure to heat leads to phase transformations in the bulk of the material, such as the formation of oxides of the surface contacting with the air (owing to

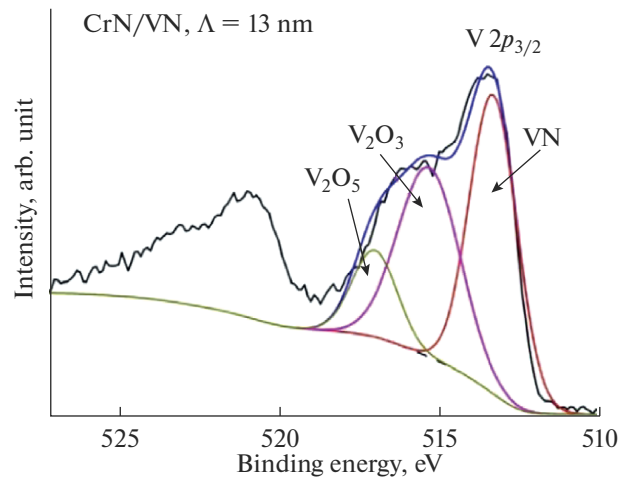


**Fig. 19.**  $V 2p_{3/2}$  XPS spectra of the wear products of the CrN/VN coating with a modulation period of  $\Lambda = 13$  nm [71].

the diffusion of oxygen atoms) and diffusionless recrystallization processes. The growing demand for the industrial use of protective multilayer coatings capable of operating under the action of high temperature loads causes an urgent need for new studies in this field.

It is well known that the mechanical and tribological properties of multilayer nitride coatings largely depend on modulation period  $\Lambda$  [77, 78]. A comparative analysis of CrAlN/TiN and CrAlN/ZrN functional coatings ( $\Lambda = 2, 7,$  and  $9$  nm, respectively) showed a tendency to improving the mechanical and thermal properties with decreasing modulation period  $\Lambda$  [79]. In this context, of particular interest is [80], the authors of which studied the mechanical and thermal properties of a CrAlN/ZrN coating at  $\Lambda \sim 5$  nm.

Figure 20 shows results of measurements of hardness ( $H$ ) for a multilayer CrAlN/ZrN coating ( $\Lambda = 5$  nm) and a CrAlN/ZrN reference sample ( $\Lambda = 9$  nm). The hardness of the CrAlN/ZrN coating with  $\Lambda = 5$  nm is significantly higher than that of the reference sample (30.7 against 27.4 GPa), a finding that is attributed to the switching from the nonepitaxial to local epitaxial growth of the layers with a decrease in the modulation period to 5 nm. An improvement of the mechanical and tribological characteristics of the multilayer coatings with the epitaxial growth of the layers is caused by a combination of different hardening mechanisms (the Hall–Petch effect, the Koehler model, the formation of internal stresses, the dislocation migration effect, etc.) [81–84]. The elastic modulus for the CrAlN/ZrN coatings with  $\Lambda = 5$  and 9 nm is  $400.3 \pm 13.1$  and  $395.9 \pm 10.5$  GPa, respectively. Hence, at  $\Lambda = 5$  nm, the  $H^3/E^2$  value of the coating is higher ( $\sim 0.18$ ) than that at  $\Lambda = 9$  nm ( $\sim 0.13$ ). This finding suggests that CrAlN/ZrN exhibits a higher wear resistance [85].

Vacuum annealing of the multilayer CrAlN/ZrN coatings ( $\Lambda = 5$  and  $9$  nm) to  $T_{\text{ann}} = 700^\circ\text{C}$  causes a slight decrease in hardness owing to the reduction and internal stress relaxation processes. A further increase in the annealing temperature to  $1100^\circ\text{C}$  leads to the formation of w-AlN and a decrease in the nitrogen content in the CrAlN layers, which in turn leads to a continuous decrease in hardness. Thus, the effect of high temperatures (up to  $1000^\circ\text{C}$ ) on the CrAlN/ZrN coating with  $\Lambda = 5$  nm does not lead to a significant change in hardness. The local epitaxial growth of layers in a multilayer system hinders the formation of cleavages and cracks and thereby increases the adhesion strength of the coating to the substrate. The adhesion strength of the CrAlN/ZrN coatings with  $\Lambda = 9$  and  $5$  nm corresponds to  $74$  and  $86$  N, respectively.

The authors of [80] assert that a decrease in the modulation period of layers in the CrAlN/ZrN coating positively affects the oxidation resistance owing to the effect of the CrAlN layers on the epitaxial growth of ZrN during deposition. In addition, the interfaces of individual layers can slow down the diffusion of oxygen atoms deep into the coating and thereby improve the protective properties of the multilayer system. It should be noted that an increase in the number of interfaces between the layers in CrAlN/ZrN with  $\Lambda = 5$  nm also leads to an increase in the oxidation resistance of the coating [86].

Wear-resistant binary coatings, which are conventionally used for hardening parts of mechanisms operating under conditions of dry friction and high temperatures, have a certain degree of porosity; therefore, they are not corrosion-resistant. A growing need for the development of novel solutions and improvement of the existing approaches to increasing the corrosion resistance of materials is observed in medicine, shipbuilding, and the industry of artificial water areas [87, 88]. An effective method for the formation of nonporous wear- and corrosion-resistant coatings is the design of nanostructured multilayer systems. Single-layer coatings based on chromium nitride (CrN) and aluminum-doped coatings (Cr–Al–N) have been quite thoroughly studied because they have excellent physicomachanical characteristics, such as hardness, wear resistance, high thermal stability, and corrosion resistance [89–92]. Since zirconium is commonly used as an intermediate layer [93, 94] to increase the corrosion resistance and mechanical and antifriction properties of coatings, the multilayer Zr/CrN system should be analyzed in detail.

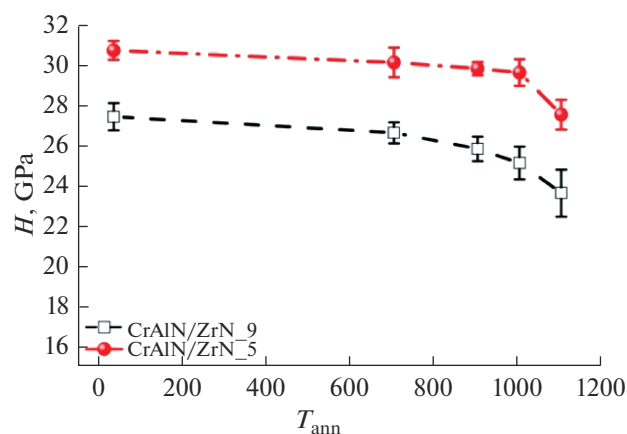


Fig. 20. Results of measurements of hardness  $H$  of the CrAlN/ZrN coating ( $\Lambda = 5, 9$  nm) after thermal annealing in a vacuum [80].

The authors of [95] analyzed the effect of the modulation ratios of layers in the Zr/CrN system on the structure, tribological properties, and corrosion resistance of the coating. Zr/CrN condensates were prepared by cathodic-arc deposition. The modulation ratios of layers for a set of Zr/CrN coatings are listed in Table 2. The thickness of the bilayers was varied in a range of about  $160$ – $370$  nm.

To analyze the corrosion resistance of the coatings, the authors of [95] prepared a solution simulating sea water in accordance with ASTM D 1141-98. The electrochemical behavior of the multilayer system was studied by the potentiodynamic method at room temperature. Figure 21 shows polarization curves of Zr/CrN coatings and an uncoated 316L substrate used as a reference sample. According to the polarization curves, corrosion potential ( $E_{\text{corr}}$ ) and corrosion current-density values ( $i_{\text{corr}}$ ) were determined (Table 2). Compared with the uncoated substrate, the NM1–NM4 samples have higher  $E_{\text{corr}}$  values and lower  $i_{\text{corr}}$  values, a finding that indicates a fairly high corrosion resistance of the coatings. The current corrosion density of the multilayer coatings is inversely proportional to an increase in the  $t_{\text{CrN}}/t_{\text{Zr}}$  modulation ratio; this fact suggests that the NM4 sample ( $t_{\text{CrN}}/t_{\text{Zr}} \sim 3.3 : 1$ ) has the best corrosion resistance of all the coatings discussed in this study.

Typically, nitride coatings based on zirconium and other elements of the extended group of refractory

Table 2. Modulation ratio of layers and potentiodynamic characteristics of Zr/CrN coatings [95]

Sample number	NM1	NM2	NM3	NM4	Substrate
$E_{\text{corr}}$ , V	–0.3	–0.25	–0.25	–0.25	–0.45
$i_{\text{corr}}$ , $\times 10^{-7}$ A/cm <sup>2</sup>	1.4	0.71	0.64	0.5	20.3
Modulation ratio of layers $t_{\text{CrN}}/t_{\text{Zr}}$	$\sim 0.9 : 1$	$\sim 1.7 : 1$	$\sim 2.5 : 1$	$\sim 3.3 : 1$	

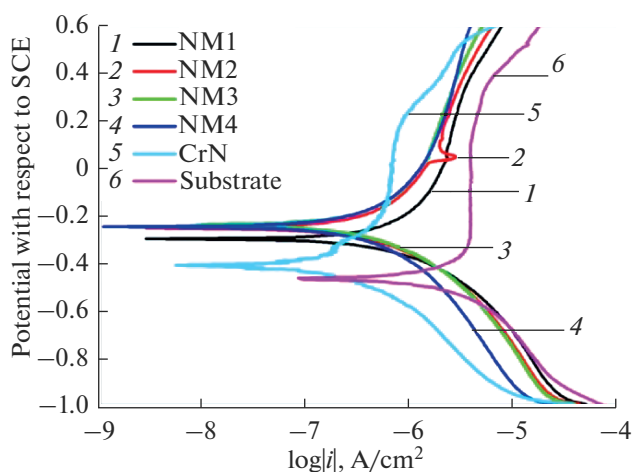


**Fig. 21.** Potentiodynamic polarization curves for a set of Zr/CrN coatings and a steel substrate [95].

metals are relatively inert to chemical attacks owing to a higher position in the electrochemical series [96, 97]. An advantage of multilayer coatings lies in the presence of interfaces between the layers, which act as a barrier to the diffusion of the electrolyte to the substrate [98, 99]. For most multilayer systems, an increase in the number of interfaces between the layers leads to an increase in corrosion resistance; however, in this case, although the NM1 coating has the largest number of interfaces, it exhibits a relatively low corrosion resistance [63, 100, 101]. Since the coatings have a certain degree of porosity and are characterized by the presence of dispersed particles on the surface, a contact with an aggressive aqueous medium stimulates the local galvanic corrosion process. The spherical shape of the particles suggests that they were apparently formed from the droplet fraction of an arc discharge plasma. The irregularly shaped particles are based on solid microparticles of the cathode, which can be emitted owing to the occurrence of thermoelastic stresses in the region of the cathode spot. The dispersed particles can form local galvanic pairs between one particle as an anode and another particle as a cathode. The authors of [95] assert that the NM1 sample has a high degree of surface roughness owing to the abundant droplet fraction; it is this factor that leads to a vigorous galvanic corrosion process. In addition, the interfaces between the layers do not hinder the formation of micropores in the coating [98]. An increase in the thickness of CrN layers not only provides a decrease in the galvanic cells between the layers, but also impedes the charge transfer and thereby improves the corrosion resistance of the multilayer Zr/CrN coatings. Hence, the multilayer systems with the highest modulation ratio ( $t_{\text{CrN}}/t_{\text{Zr}} \sim 3.3 : 1$ ) exhibit the best corrosion resistance.

The use of nanocomposite TiAlN/ZrN coatings to improve the corrosion resistance of spheroidal-graph-

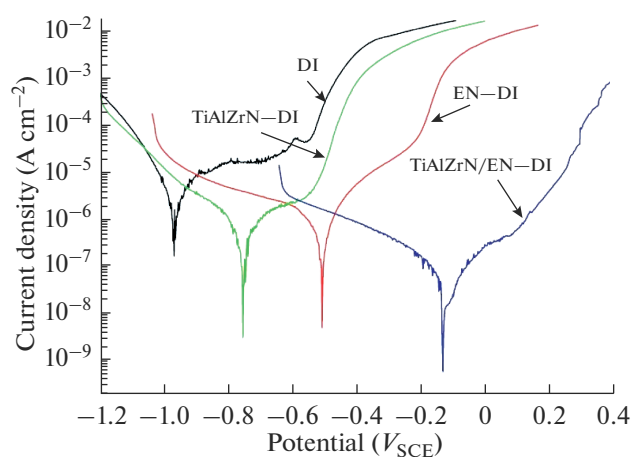


**Fig. 22.** Polarization curves for uncoated DI and the EN-DI, TiAlZrN-DI, and TiAlZrN/EN-DI samples in a 3.5% NaCl solution.

ite cast iron was analyzed in [102]. For a number of samples, electroless nickel (EN) plating was conducted to form an intermediate layer between the substrate and the coating. Nickel plating of ductile iron (DI) is aimed at improving the protective properties of functional coatings exposed to the action of aggressive media and erosion. The corrosion resistance of vacuum condensates and the EN layer was analyzed by the potentiodynamic method at room temperature (25°C). Potentiodynamic polarization measurements were conducted in a 3.5% NaCl solution. Figure 22 shows the polarization curves for corrosion potential ( $E_{\text{corr}}$ ) and corrosion current density values ( $i_{\text{corr}}$ ). For all the three deposited coatings, an increase in the  $E_{\text{corr}}$  value was observed; this fact indicates an improvement in their corrosion resistance compared with that of the uncoated DI. Thus, for DI, the  $E_{\text{corr}}$  value was  $-0.959 V_{\text{SCE}}$ , while, for the TiAl/Zr-DI and TiAlZr/EN coatings, the corrosion potential was at a level of  $-0.750$  and  $-0.117 V_{\text{SCE}}$ , respectively.

Corrosion current density was calculated using the Tafel equation [103]. The derived values also confirm an improvement in the corrosion resistance of the samples with a functional coating. According to the results, the  $i_{\text{corr}}$  value of DI is  $2.2 \times 10^{-6} \text{ A/cm}^2$ , which is significantly larger than the value of the coated samples. The corrosion current for the multilayer TiAlZrN-DI and TiAlZrN/EN-DI coatings is  $4.3 \times 10^{-7}$  and  $5.4 \times 10^{-8} \text{ A/cm}^2$ , respectively.

After polarization measurements, the sample surface was studied by scanning electron microscopy. According to the micrographs in Fig. 23a, the Fe matrix around the graphite particle was destroyed by corrosion, an event that is characteristic of spheroidal-graphite cast iron. After the deposition of a multilayer TiAl/Zr-DI coating, the area of corrosion damage became significantly smaller (Fig. 23c) owing to the



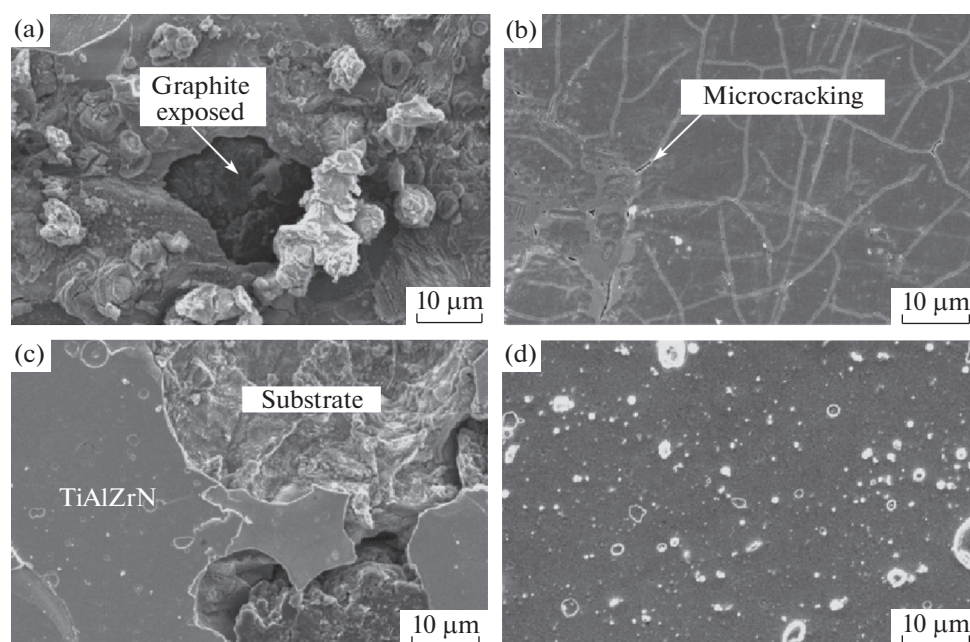


**Fig. 23.** SEM image of the surface after the polarization test: (a) uncoated DI and (b) the EN–DI, (c) TiAlZrN–DI, and (d) TiAlZrN/EN–DI samples.

layered structure of the multilayer system. However, the authors of [102] assert that the TiAlZrN/EN–DI coating has the best corrosion resistance owing to the formation of a transition layer by EN plating. Figure 23d shows shallow local corrosion traces and the absence of microcracks. In addition, the deposition of an EN transition layer provides an improvement of the adhesion strength of the coating.

In the case of deposition only of a 25- $\mu\text{m}$ -thick monolithic EN layer, a large number of through-thickness microcracks are formed on the surface of the deposited layer. Owing to these microcracks, an aggressive medium can affect the material to be protected. According to X-ray diffraction analysis, the EN layer has an entirely amorphous structure, whereas TiAlZrN consists of TiAlN and ZrN crystalline phases. Thus, it is suggested that a duplex multilayer TiAlZrN/EN–DI coating may improve the corrosion and erosion resistance of spheroidal-graphite cast iron.

## CONCLUSIONS

This review has summarized the results of studies of nanostructured multilayer coatings based on an extended group of refractory metals. Particular attention has been paid to the effect of the periodic layered structure on the tribological properties, thermal stability, and corrosion resistance of multilayer nitride coatings. Mechanisms of dry wear of multilayer systems with different modulation periods ( $\Lambda$ ) in a temperature range of 0–1100°C have been discussed. The dependence of the resulting structure and the respec-

tive characteristics of the coatings on the conditions of their deposition has been shown.


It has been found that the mechanical, tribological, and tribotechnical characteristics of multilayer systems are significantly affected by both the deposition conditions and the structural features of the coatings, namely, the period and ratio of the modulation wave. Since the studied physical process is multifactor in nature, it is impossible to establish a common general law governing the choice of the technological parameters of deposition and the optimum modulation period ( $\Lambda$ ); therefore, to achieve the desired results in each particular case, it is necessary to optimize the coating deposition process. In general, a decrease in the layer thickness to nanoscale sizes causes an improvement of the above properties owing to an increase in the number of interfaces between the layers, which act as a barrier to the propagation of microcracks arising under the action of a load during friction. Under these conditions, degradation is localized within the individual layers, and it is this feature that provides an improvement of the tribological characteristics of the coatings and their performance characteristics.

Functional coatings with an adaptive friction mechanism and processes that occur in the contact area have been analyzed separately. The antifriction properties of these materials are improved owing to the formation of molybdenum and vanadium oxides (particularly  $\text{V}_2\text{O}_3$  and  $\text{V}_2\text{O}_5$ ) respectively. An oxide film on the surface of functional coatings plays the role of a lubricant and thereby decreases the coefficient of fric-

tion and the volume of the worn material. Adaptive wear-resistant coatings completely fulfill their potential under extreme tribological conditions because the active phase of formation of a tribofilm begins after an increase in temperature caused by the mechanical interaction with the counterbody.

An increase in the number of interfaces between monolayers is a necessary condition for an increase in the thermal stability and corrosion resistance of multilayer coatings based on refractory elements because the barrier produced by them can slow down the diffusion of oxygen atoms and aggressive media deep into the coating and thus prevent the degradation of the coating and the material to be protected.

## REFERENCES

- Hovsepian, P.E.H., Lewis, D.B., and Munz, W.D., *Surf. Coat. Technol.*, 2000, vols. 133–134, p. 166.
- Nordin, M., Larsson, M., and Hogmark, S., *Wear*, 1999, vol. 232, p. 221.
- Nordin, M., Larsson, M., and Hogmark, S., *Surf. Coat. Technol.*, 1998, vol. 106, p. 234.
- Pogrebnyak, A., Pshyk, A., Coy, E., et al., *Phys. Met. Metallogr.*, 2016, vol. 117, no. 10, p. 990.
- Pogrebnyak, A.D., Bondar, O.V., Abadias, G., et al., *Acta Phys. Pol., A*, 2015, vol. 128, no. 5, p. 836.
- Pogrebnyak, A.D., Maksakova, O., Kozak, C., et al., *Przegl. Elektrotech.*, 2016, vol. 2016, no. 8, p. 180.
- Pogrebnyak, A.D., Yakushchenko, I.V., Bondar, O.V., et al., *Phys. Solid State*, 2015, vol. 57, no. 8, p. 1559.
- Turbin, P.V., Farenik, V.I., Tseluiko, A.F., et al., *Prom. Tekhnol.*, 2003, vol. 5, no. 5, p. 37.
- An, J. and Zhang, Q.Y., *Mater. Charact.*, 2007, vol. 58, p. 439.
- Nordin, M. and Ericson, F., *Thin Solid Films*, 2001, vol. 385, nos. 1–2, p. 174.
- Ma, G., Lin, G., Gong, S., Liu, X., Sun, G., and Wu, H., *Vacuum*, 2013.
- Bushan, B. and Gupta, B., *Handbook of Tribology*, New York: McGraw Hill, 1991, p. 57.
- Kim, S.K. and Cha, B.C., *Thin Solid Films*, 2005, vol. 475, p. 202.
- Leng, Y.X., Sun, H., Yang, P., et al., *Thin Solid Films*, 2000, vols. 398–399, p. 471.
- Shin, C.S., Kim, Y.W., Gall, D., Greene, J.E., and Petrov, I., *Thin Solid Films*, 2002, vol. 402, p. 172.
- Lee, G.R., Kim, H., Choi, H.S., and Lee, J.J., *Surf. Coat. Technol.*, 2007, vol. 201, p. 5207.
- Liu, K., Lee, J., and Wu, F., *Surf. Coat. Technol.*, 2014, vol. 2, p. 123.
- Zhang, Z.G., Rapaud, O., Allain, N., et al., *Appl. Surf. Sci.*, 2009, vol. 255, p. 4020.
- Pelleg, J., Zevin, L.Z., Lungo, S., and Croitoru, N., *Thin Solid Films*, 1991, vol. 197, p. 117.
- Rizzo, A., Signore, M.A., Penza, M., et al., *Thin Solid Films*, 2006, vol. 515, p. 500.
- Beresnev, V.M., Sobol', O.V., Pogrebnyak, A.D., et al., *Tech. Phys. Lett.*, 2016, vol. 42, no. 5, p. 532.
- Klepikov, V.F., Lonin, Yu.F., Lytvynenko, V.V., et al., *Probl. At. Sci. Technol., Ser.: Nucl. Phys. Invest.*, 2008, vol. 50, no. 5, p. 91.
- Batracov, A.B., Bazaleev, M.I., Donets, S.E., et al., *Probl. At. Sci. Technol., Ser.: Nucl. Phys. Invest.*, 2013, vol. 88, no. 6, p. 225.
- Pogrebnyak, A.D., Ivasishin, O.M., and Beresnev, V.M., *Usp. Fiz. Met.*, 2016, vol. 17, p. 1.
- Wadsworth, I., Smith, I.J., Donohue, L.A., and Münz, W.D., *Surf. Coat. Technol.*, 1997, vols. 94–95, p. 315.
- Lembke, M.I., Lewis, D.B., and Münz, W.D., *Surf. Coat. Technol.*, 2000, vol. 125, p. 263.
- Harris, S.G., Doyle, E.D., Vlasveld, A.C., et al., *Wear*, 2003, vol. 254, p. 723.
- Yamamoto, K., Sato, T., Takahara, K., and Hanaguri, K., *Surf. Coat. Technol.*, 2003, vols. 174–175, p. 620.
- Chang, Y., Wang, D., and Hung, C., *Surf. Coat. Technol.*, 2005, vol. 200, p. 1702.
- Yashar, P.C. and Sproul, W.D., *Vacuum*, 1999, vol. 55, p. 179.
- Pogrebnyak, A.D. and Goncharov, O.  *Metallofiz. Noveishie Tekhnol.*, 2016, vol. 38, no. 1, p. 1145.
- Dolique, V., Thomann, A.-L., Brault, P., et al., *Mater. Chem. Phys.*, 2009, vol. 117, no. 1, p. 142.
- Dolique, V., Thomann, A.-L., Brault, P., et al., *Surf. Coat. Technol.*, 2010, vol. 204, p. 1989.
- Tsai, M.H., Wang, C.W., Tsai, C.W., et al., *J. Electrochem. Soc.*, 2011, vol. 158, no. 11, p. 1161.
- Ranganathan, S., *Curr. Sci.*, 2003, vol. 85, no. 10, p. 1404.
- Pogrebnyak, A.D., Bor'ba, S.O., Kravchenko, Y.O., et al., *J. Superhard Mater.*, 2016, vol. 38, no. 6, p. 393.
- Pogrebnyak, A.D., Yakushchenko, I.V., Bondar, O.V., et al., *J. Alloys Compd.*, 2016, vol. 679, p. 155.
- Pogrebnyak, A.D., Yakushchenko, I.V., Bondar, O.V., et al., *Tech. Phys. Lett.*, 2015, vol. 41, no. 11, p. 1054.
- Komarov, F.F., Pogrebnyak, A.D., and Konstantinov, S.V., *Tech. Phys.*, 2015, vol. 60, no. 10, p. 1519.
- Pogrebnyak, A.D., Yakushchenko, I.V., Sobol', O.V., et al., *Tech. Phys.*, 2015, vol. 60, no. 8, p. 1176.
- Pogrebnyak, A.D., Eyidi, D., Abadias, G., et al., *Int. J. Refract. Met. Hard Mater.*, 2015, vol. 48, p. 222.
- Pogrebnyak, A.D., Abadias, G., Bondar, O., et al., *Acta Phys. Pol., A*, 2014, vol. 125, p. 1280.
- Beresnev, V.M., Sobol', O.V., et al., *Tech. Phys. Lett.*, 2016, vol. 42, no. 5, p. 532.
- Nyemchenko, U.S., Beresnev, V.M., Sobol, O.V., et al., *PAST*, 2016, vol. 101, no. 1, p. 112.
- Maksakova, O.V., Grankin, S.S., Bondar, O.V., et al., *J. Nano- Electron. Phys.*, 2015, vol. 7, no. 4, p. 04098-1.
- Pshyk, A.V., Coy, L.E., Yate, L., et al., *Mater. Des.*, 2016, vol. 94, p. 230.
- Pogrebnyak, A.D., Bondar, O., Abadias, G., et al., *Ceram. Int.*, 2016, vol. 42, no. 10, p. 11743.
- Kravchenko, Ya.O., Maksakova, O., Drodziel, P., and Loboda, V., *High Temp. Mater. Processes*, 2016, vol. 20, no. 1, p. 85.
- Pogrebnyak, A.D., Bagdasaryan, A.A., Beresnev, V.M., et al., *Ceram. Int.*, 2017, vol. 43, no. 1, p. 771.

50. Lackner, J., Waldhauser, W., Ebner, R., et al., *Thin Solid Films*, 2004, vols. 453–454, p. 195.
51. Pogrebnjak, A.D., Yakushchenko, I.V., Bondar, O.V., et al., *Phys. Solid State*, 2015, vol. 57, no. 8, p. 1559.
52. Ou, Y.X., Lin, J., Che, H.L., et al., *Thin Solid Films*, 2015, vol. 594, p. 1.
53. Archard, J.F., *J. Appl. Phys.*, 1953, vol. 24, p. 981.
54. Leyland, A. and Matthews, A., *Wear*, 2000, vol. 246, p. 1.
55. Yashar, P.C. and Sproul, W.D., *Vacuum*, 1999, vol. 55, p. 179.
56. Lehoczky, S.L., *J. Appl. Phys.*, 1978, vol. 49, p. 5479.
57. Chu, X. and Barnett, S.A., *J. Appl. Phys.*, 1995, vol. 77, p. 4403.
58. Ou, Y.X., Lin, J., Che, H.L., et al., *Surf. Coat. Technol.*, 2016, vol. 276, p. 152.
59. Voevodin, A.A. and Zabinski, J.S., *Thin Solid Films*, 2000, vol. 370, p. 223.
60. Basnyat, B., Luster, B., Kertzman, Z., et al., *Surf. Coat. Technol.*, 2007, vol. 202, p. 1011.
61. Kelly, P.J., Li, H., Benson, P.S., et al., *Surf. Coat. Technol.*, 2010, vol. 205, p. 1606.
62. Stone, D., Migas, J., Martini, A., et al., *Surf. Coat. Technol.*, 2012, vol. 206, p. 4316.
63. Wang, T., Zhang, G., and Jiang, B., *Appl. Surf. Sci.*, 2016, vol. 363, p. 217.
64. Bai, L., Zhu, X., Xiao, J., and He, J., *Surf. Coat. Technol.*, 2007, vol. 201, p. 5257.
65. Gassner, G., Mayrhofer, P.H., Kutschej, K., and Mitterer, C., *Surf. Coat. Technol.*, 2006, vol. 201, p. 3335.
66. Suszko, T., Gulbiński, W., and Jagielski, J., *Surf. Coat. Technol.*, 2005, vol. 194, p. 319.
67. Wang, T., Zhang, G., Liu, Z., and Jiang, B., *Ceram. Int.*, 2015, vol. 41, p. 7028.
68. Qiu, Y., Zhang, S., Li, B., et al., *Surf. Coat. Technol.*, 2013, vol. 231, p. 357.
69. Lu, Y.H., Shen, Y.G., Zhou, Z.F., and Li, K.Y., *Wear*, 2007, vol. 262, p. 1372.
70. Mayrhofer, P.H., Hovsepian, P.E.H., Mitterer, C., and Münz, W.-D., *Surf. Coat. Technol.*, 2004, vol. 341, p. 177.
71. Willmann, H., Beckers, M., Giuliani, F., et al., *Scr. Mater.*, 2007, vol. 57, p. 1089.
72. Wuhner, R. and Yeung, W.Y., *Scr. Mater.*, 2004, vol. 50, p. 1461.
73. Li, Z., Munroe, P., Jiang, Z.T., et al., *Acta Mater.*, 2012, vol. 60, p. 5735.
74. Knotek, O., Löffler, F., and Scholl, H.-J., *Surf. Coat. Technol.*, 1991, vol. 45, p. 53.
75. Reiter, A.E., Derflinger, V.H., Hanselmann, B., et al., *Surf. Coat. Technol.*, 2005, vol. 200, p. 2114.
76. Lin, J., Mishra, B., Moore, J.J., and Sproul, W.D., *Surf. Coat. Technol.*, 2008, vol. 202, p. 3272.
77. Yashar, P.C. and Sproul, W.D., *Vacuum*, 1999, vol. 55, p. 179.
78. Helmersson, U., Todorova, S., Barnett, S.A., et al., *J. Appl. Phys.*, 1987, vol. 62, p. 481.
79. Chen, L., Xu, Y.X., and Zhang, L.J., *Surf. Coat. Technol.*, 2016, vol. 285, p. 146.
80. Li, Chen and Xu, Yu.X., *Mater. Des.*, 2016, vol. 106, p. 1.
81. Koehler, J.S., *Phys. Rev. B*, 1970, vol. 2, p. 547.
82. Anderson, P.M. and Li, C., *Nanostruct. Mater.*, 1995, vol. 5, p. 349.
83. Kato, M., Mori, T., and Schwartz, L.H., *Acta Metall.*, 1980, vol. 28, p. 285.
84. Cammarata, R.C., *Scr. Metall.*, 1986, vol. 20, p. 479.
85. Leyland, A. and Matthews, A., *Wear*, 2000, vol. 246, p. 1.
86. Chen, H.W., Chan, Y.C., Lee, J.W., and Duh, J.G., *Surf. Coat. Technol.*, 2010, vol. 205, p. 1189.
87. Totolin, V., Pejaković, V., Csanyi, T., et al., *Mater. Des.*, 2016, vol. 104, p. 10.
88. Shan, L., Wang, Y., Li, J., et al., *Tribol. Int.*, 2015, vol. 82, p. 78.
89. Zhang, M., Li, M.-K., Kim, K.H., and Pan, F., *Appl. Surf. Sci.*, 2009, vol. 255, p. 9200.
90. Polcar, T., Parreira, N.M.G., and Novak, R., *Surf. Coat. Technol.*, 2007, vol. 201, p. 5228.
91. Jung, M.J., Nam, K.H., Jung, Y.M., and Han, J.G., *Surf. Coat. Technol.*, 2003, vol. 171, p. 59.
92. Djouadi, M.A., Nouveau, C., Beer, P., and Lambertin, M., *Surf. Coat. Technol.*, 2000, vols. 133–134, p. 478.
93. Verma, N. and Jayaram, V., *J. Mater. Res.*, 2013, vol. 28, p. 3146.
94. Kim, S.M., Kim, B.S., Kim, G.S., et al., *Surf. Coat. Technol.*, 2008, vol. 202, p. 5521.
95. Guan, X., Wang, Y., Zhang, G., et al., *Tribol. Int.*, 2017, vol. 106, p. 78.
96. Wang, H.W., Stack, M.M., Lyon, S.B., et al., *Surf. Coat. Technol.*, 2000, vol. 126, p. 279.
97. Pejaković, V., Totolin, V., Göcerler, H., et al., *Tribol. Int.*, 2015, vol. 91, p. 267.
98. Song, G.-H., Yang, X.-P., Xiong, G.-L., et al., *Vacuum*, 2013, vol. 89, p. 136.
99. Creus, J., Top, E.H., Savall, C., et al., *Surf. Coat. Technol.*, 2008, vol. 202, p. 4047.
100. Chipatecua, Y.L., Olaya, J.J., and Arias, D.F., *Vacuum*, 2012, vol. 86, p. 1393.
101. Aouadi, S.M., Luster, B., Kohli, P., et al., *Surf. Coat. Technol.*, 2009, vol. 204, p. 962.
102. Lin, C., Hsu, C., Cheng, Y., et al., *Appl. Surf. Sci.*, 2015, vol. 324, p. 13.
103. Rocchini, G., *Corros. Sci.*, 1995, vol. 37, p. 987.

Translated by M. Timoshinina